

Margarida Vaz de Vasconcelos da Silva Laires BSc in Micro and Nanotechnology Engineering

Sensor System for Padel/Tennis Racket: Acquiring and Analysing Performance Data for Enhanced Gameplay

Master in Micro and Nanotechnology Engineering NOVA University Lisbon September 2024



DEPARTMENT OF MATERIALS SCIENCE

Sensor System for Padel/Tennis Racket: Acquiring and Analysing Performance Data for Enhanced Gameplay

Margarida Vaz de Vasconcelos da Silva Laires

BSc in Micro and Nanotechnology Engineering

Adviser: Dr. Felisberto Pereira

Senior Researcher, AlmaScience Association

Co-adviser: Prof. Dr. Rui Igreja

Associate Professor, NOVA School of Science and Technology

Examination Committee:

Chair: Prof. Dr. Hugo Águas

Associate Professor, NOVA School of Science and Technology

Rapporteurs: Prof. Dra. Joana Vaz Pinto

Associate Professor, NOVA School of Science and Technology

Adviser: Dr. Felisberto Pereira

Senior Researcher, AlmaScience Association

Master in Micro and Nanotechnology Engineering NOVA University Lisbon September 2024

Sensor System for Padel/Tennis Racket: Acquiring and Analysing Performance Data for Enhanced Gameplay
Copyright © Margarida Laires, NOVA School of Science and Technology, NOVA University Lisbon. The NOVA School of Science and Technology and the NOVA University Lisbon have the right, perpetual and without geographical boundaries, to file and publish this dissertation through printed copies reproduced on paper or on digital form, or by any other means known or that may be invented, and to disseminate through scientific repositories and admit its copying and distribution for non-commercial, educational or research purposes, as long as credit is given to the author and editor. This document was created with Microsoft Word text processor and the NOVAthesis Word template [1].

ACKNOWLEDGMENTS

First and foremost, I would like to express my gratitude to NOVA School of Science and Technology and its staff for guiding me through an enriching academic journey and the wealth of knowledge I gained. A special thank you to Rodrigo Martins and Elvira Fortunato for their dedication to shaping my program and their unwavering commitment to research.

To my supervisors Felisberto Pereira and Professor Rui Igreja a special "Thank You" for all the support throughout these months and for allowing me to have a challenging experience. To all the staff at AlmaScience, especially Wilson, Inês, Mariana and Tomás, for all the help, ideas and, particularly, for explaining every single question I had regarding this work.

To my peers in MIEMN, thank you for making this journey what it was. Without you, these last 5 years would've been way harder – no doubt about it. To the "Chá no Copo" group, now "Sotão da CoPe", thanks for making me laugh when I least expected, for taking my mind of everything and, especially, for paving the way for Praxe de Nano. You guys are absolute legends and the best group I could've asked for. To Matita, you are the most brilliant, mesmerizing, inspiring (yet stressed) person I've ever met. Thank you for being my partner all these years, for calling me every 10 minutes to make sure that we finished the work and for always checking on me. To my little "son", Leo, for always being the yin to my yang, trying to keep me calm and collected and for believing in me even when I didn't. To Calado aka Béa, who never let me give up, even when I didn't have any strength, you took the wheel and guided me through these years. To Gótumu, for being the chaotic little brother in my life, for all deep talks from FCT to 7rivers and for being the funniest person I met in Nano. To my two little mini me's, Rita and Çara, thank you for making me feel ancient (but always wanted), believing in me and for holding down the fort after I left (ps: a shoutout to Nónó for actually reading this work and rating it). To Edu, thank you for being the person I could always turn to when things went wrong—you always knew exactly what to say. To Tiago, Bianca e Inês, thanks for keeping me company and stress-free. To Hervé, for sharing most of the last 6 months with me and helping me when every single thing that seemed impossible. To my little "daughter", Catarina, for trying to push me out of my comfort zone and live life to the fullest. To Matilde, my fada das bubas, thank you for being my study buddy and for that contagious energy that burst out of your tiny body. To Raquel, we're connected on a whole other level, thank you for all the motivational words and for understanding me without even needing to say anything. To Mogli, for being my partner in crime, for always having my back and for enduring my anger issues during training.

I also want to thank my family - every single one of you shaped me into the person I am today. When I become a Master, know that it was because of each and every one of you. Together and individually, you've given me the courage to face every challenge and finish what I've started.

To Manel and Nena, my siblings, I love you with all my heart. You've known me the longest and shared basically my entire life with me. Thank you for the ups and downs, for sticking with me through thick and thin, for never stop believing in me and, most of all, for being my best friends. Without you, I would never have accomplished what I did. For that and so much more, THANK YOU. I also want to thank tia Dina, who has been like a second mom to me since I was a baby.

To my soulmate, Mariana, no words can truly express my gratitude towards you. You are the most amazing person I know, and I feel honoured to have shared the last 5 years with you. Thank you for all the talks, the "suck it up and just do it" moments, the wise words and for always being the voice

of reason. You kept me going through these last few months and never let me fall. You are my biggest supporter and I'm beyond grateful to be able to share the rest of my life with you.

To my sister, Nô, for being my role model. You've paved the way I want to follow and I'm your biggest fan (and also your biggest hater, but you know how it is). Thank you for being the best big sister I could have ever asked for and for always reassuring me that everything would be okay. To my *guistosinhas*, thank you for putting a smile on my face and filling my heart with love every time I think of you. To my mummy, thank you for raising me, for loving me, for defending me and teaching me everything you know. To my papi, thank you for loving me, for pushing me to be my best self, for fighting for my education and for being my personal chatgpt. You guys are both my rocks and I know that everything I've achieved is because of you both.

This work was financed by national funds from FCT - Fundação para a Ciência e a Tecnologia, I.P., in the scope of the projects LA/P/0037/2020, UIDP/50025/2020 and UIDB/50025/2020 of the Associate Laboratory Institute of Nanostructures, Nanomodelling and Nanofabrication – i3N)

"To invent, you need a good imagination and a pile of junk" (Thomas Edison)

ABSTRACT

Wearables have become a key focus in technology, particularly in entertainment, healthcare and sports, largely driven by advances in microelectronics and functional materials. In sports, these devices allow real-time performance tracking, helping athletes improve their results. However, the lack of wearable technology research in padel and tennis highlights the need to develop solutions that can measure parameters such as hand position and strength.

This work aims to develop an innovative smart grip for padel and tennis rackets, designed to gather data on the player's grip, offering insights for performance optimization. Three different grip prototypes were fabricated using different functional materials: 1) paper with Velostat, 2) cork with Velostat and 3) paper with hydrogel. Each grip was tested in a pressure machine and through player-interface evaluations.

The paper with Velostat grip, with silver screen-printed electrodes and Velostat as the piezoresistive material, maintained consistent output under prolonged force and repeatable output signals during fast force cycles, demonstrating strong potential for this application. The sensor's sensibility is (-1 \pm 0.5) MPa⁻¹ for low pressures and (-1 \pm 0.2) MPa⁻¹ for high pressures . The paper substrate exhibited wear after testing.

The cork with Velostat grip, designed to improve durability, provided clear force discrimination in machine tests and consistent output signals under prolonged force and fast force cycles. During player-interface evaluations, the sensor demonstrated limited responsiveness. However, retesting with a 1 k Ω bias resistor, improved its performance, resulting in more noticeable voltage changes and, hence, better sensitivity.

The paper with hydrogel grip, an eco-friendlier option, utilized hydrogel droplets as the active material. This grip responded to distinct force values, demonstrating a sensibility of (-9 \pm 1) MPa⁻¹ for low pressures and (-4 \pm 0.4) MPa⁻¹ for high pressures. Although it exhibited slower recovery times under sustained force, its responsiveness to fast force cycles highlights its potential for dynamic performance monitoring.

Overall, the cork with Velostat grip emerged as the most viable option, delivering exceptional performance and durability throughout testing. With further research, this innovation stands to revolutionize the wearable industry in padel and tennis, offering a unique level of insight into the player's performance.

Keywords: Enhancement gameplay, pressure sensor array, racket sports, smart grip, Velostat

RESUMO

Os *wearables* tornaram-se um foco principal na tecnologia, particularmente no entretenimento, na saúde e no desporto, impulsionados principalmente pelos avanços na microeletrónica e materiais funcionais. No desporto, estes dispositivos permitem a monitorização do desempenho do atleta em tempo real, melhorando, assim, os seus resultados. No entanto, a falta de investigação em tecnologia *wearable* no padel e no ténis destaca a necessidade de desenvolver soluções que possam medir parâmetros como a posição e a força de preensão manual.

Este trabalho visa desenvolver uma *smart grip* inovadora para raquetes de padel e ténis, projetada para recolher dados sobre a mão do jogador e fornecer informações relevantes para a otimização do seu desempenho. Foram fabricados três protótipos diferentes de *grips*, utilizando diferentes materiais funcionais: 1) papel com Velostat, 2) cortiça com Velostat e 3) papel com hidrogel. Cada *grip* foi testada numa máquina de pressão e por jogadores, imitando uma experiência em ambiente real.

A *grip* de papel com Velostat, produzida com elétrodos impressos em prata e utilizando Velostat como material piezoresistivo, manteve um sinal de saída consistente sob força prolongada e apresentou sinais de saída iguais durante os ciclos de força rápidos, demonstrando um forte potencial para esta aplicação. A sensibilidade do sensor é de (-1 ± 0.5) MPa⁻¹ para baixas pressões e (-1 ± 0.2) MPa⁻¹ para altas pressões. O substrato de papel apresentou desgaste após os testes.

A *grip* de cortiça com Velostat, projetada para melhorar a durabilidade, diferenciou níveis de força distintos nos testes da máquina de pressão, mantendo sinais de saída consistentes sob força prolongada e ciclos de força rápidos. Durante os testes com os jogadores, o sensor demonstrou uma capacidade de resposta limitada. No entanto, ao testar novamente a *grip* com uma resistência auxiliar de $1~\mathrm{k}\Omega$, o seu desempenho melhorou, resultando em alterações de tensão mais percetíveis e, consequentemente, numa melhor sensibilidade.

Para uma opção mais sustentável, produziu-se uma grip de papel com hidrogel, onde gotas de hidrogel funcionaram como material ativo. Esta grip respondeu a valores de força distintos, demonstrando uma sensibilidade de (-9 ± 1) MPa⁻¹ para pressões baixas e $(-4 \pm 0,4)$ MPa⁻¹ para pressões altas. Embora tenha apresentado tempos de recuperação mais lentos sob força prolongada, a sua capacidade de resposta a ciclos de força rápida destaca o seu potencial para monitorização de desempenho dinâmico.

Em suma, a *grip* de cortiça com Velostat surgiu como melhor opção, apresentando desempenho e durabilidade excecionais durante os testes. Estas *smart grips* inovadoras tem o potencial de revolucionar a indústria de *wearables* no padel e no ténis, oferecendo um nível único de perceção sobre o desempenho do jogador.

Palavas chave: Desportos de raquete, otimização de jogo, sensores de pressão, *smart grip*, Velostat

CONTENTS

N	10TIVAT	ION	XXV
1	INTR	RODUCTION	1
	1.1	Wearables in sports	1
	1.2	Wearables in Tennis and Padel	2
	1.3	Smart grip	3
	1.3.1	Velostat	4
	1.3.2	Cellulose-based substrates	5
	1.3.3	Hydrogels as an active layer	5
2	MAT	TERIALS AND METHODS	7
	2.1	Production of the smart grips	7
	2.1.1	Paper with Velostat Grip	7
	2.1.2	Cork with Velostat Grip	7
	2.1.3	Paper with hydrogel Grip	8
	2.2	Readout circuitry	8
	2.3	Characterization of the smart grips	9
3	RES	ULTS AND DISCUSSION	11
	3.1	Velostat	11
	3.1.1	Morphological Characterization	11
	3.2	Smart Grips	13
	3.2.1	Paper with Velostat Grip (PV grip)	14
	3.2.2	Cork with Velostat Grip (CV grip)	19
	3.2.3	Paper with Hydrogel Grip (PH grip)	27
	3.2.4	Grip comparison	31
4	Con	NCLUSIONS AND FUTURE PERSPECTIVES	35
5	ANN	IEXES	42

LIST OF FIGURES

Figure 1.1 - Schematic of the smart grip application on tennis and padel rackets	
Figure 3.2 - SEM visualization of Velostat samples displayed in Figure 3.1: a) left sample; b) right	ht
sample	
Figure 3.3 - EDS Spectra of Velostat samples displayed in Figure 3.1: a) left sample; b) right sample	
Figure 3.4 - Paper with Velostat grip: a) structure; b) grip mounted on the racket	
Figure 3.5 - Pressure machine setup and schematic for testing of the paper with Velostat grip	
Figure 3.6 -Performance of the smart grip during the Steps test: a) using a Rbias = $1 \text{ k}\Omega$; b) using	
Rbias = 330Ω .	
Figure 3.7 - Performance of the smart grip and the corresponding sensing map during the Continuou	
Pressure test	
Figure 3.8 - Performance of the smart grip and the corresponding sensing map during the Cycle 0 to 10	
N test	
Figure 3.9 - Performance of the smart grip during the Cycle 0 to 500 N test	
Figure 3.10 - Players performance with the paper with Velostat grip during player-interface evaluation	
Figure 3.11 - Cork with Velostat grip: a) structure; b) grip mounted on the racket	
Figure 3.12 - Pressure machine set up for testing of the cork with Velostat grip: a) left side of the senso	
	20
Figure 3.13 – Performance of the smart grip during the Steps test: a) left side of the sensor; b) right side	le
of the sensor.	
Figure 3.14 - Performance of the smart grip during the Continuous Pressure test: a) left side of the	
	22
Figure 3.15 - Performance of the smart grip during the Cycle 0 to 100 N test: a) left side of the senso	r;
b) right side of the sensor	
Figure 3.16 - Performance of the smart grip during the Cycle 0 to 500 N test: a) left side of the senso	r;
b) right side of the sensor	_
Figure 3.17 - Players performance with the cork with Velostat grip with a R_{bias} of 330 Ω during playe	r-
interface evaluation	
Figure 3.18 - Performance of the smart grip during the Steps test: a) left side of the sensor; b) right side	le
of the sensor	
Figure 3.19 - Performance of the smart grip during Continuous Pressure test: a) left side of the senso	
b) right side of the sensor	
Figure 3.20 - Performance of the smart grip during the Cycle 0 to 100 N test: a) left side of the senso	
b) right side of the sensor	
Figure 3.21 - Performance of the smart grip during the Cycle 0 to 500 N test: a) left side of the senso	
b) right side of the sensor	6

Figure 3.22 - Players performance with the cork with Velostat grip with a R_{bias} of 1 $k\Omega$ d	uring player-
interface evaluation.	26
Figure 3.23 - Paper with hydrogel grip: a) grip mounted on the racket; b) structure	27
Figure 3.24 - Pressure machine set up for testing of the paper with hydrogel grip	27
Figure 3.25 - Performance of the smart grip during the Steps test	28
Figure 3.26 - Performance of the smart grip during the Continuous Pressure test	29
Figure 3.27 - Performance of the smart grip during the Cycles 0 to 100 N test	30
Figure 3.28 - Performance of the smart grip during the Cycles 0 to 500 N test	30
Figure 3.29 - Players performance with the paper with hydrogel grip during player-interfac	e evaluation.
	31
Figure 3.30 - Relative resistance change for each grip, under pressures ranging from 51 kP	a to 255 kPa.
	32
Figure 5.1 - Schematic of the structure of the grips.	42
Figure 5.2- Schematic of the implementation of the grip onto the handle of the racket	43
Figure 5.3 - Schematic of the mold used for the hydrogel wells	43
Figure 5.4 - Schematic of the connections of the two parts of the paper with hydrogel grip.	44
Figure 5.5 - Schematic of the readout circuitry for signal conditioning	44
Figure 5.6 – State of the paper with Velostat grip after testing	45
Figure 5.7- State of the cork with Velostat grip after testing.	45
Figure 5.8 – State of the paper with hydrogel grip after testing	10

LIST OF TABLES

Table 3.1- Overview of the structure of the smart grips studied in this work	13
Table 3.2 – Description of users and their experience level in padel for the player-interface test	18
Table 3.3 - Average sensitivity values for the pressure ranges S_1 and S_2 of each grip	33
Table 3.4 - Overview of the smart grips studied in this work.	33
Table 5.1 – Breakdown of the estimated prices of paper with Velostat, cork with Velostat and	paper
with hydrogel grips	47

LIST OF EQUATIONS

(])	8
(2)	32



ACRONYMS

ADC Analog-to-Digital Converter

CMC Carboxymethyl Chitosan

CV grip Cork with Velostat Grip

DEMUX Demultiplexer

EDXS Energy-Dispersive X-ray Spectroscopy

Esp32 Esp32-Wroom-32U

IMU Inertial Measurement Unit

IoT Internet of Things

LC Lignin-based Carbon

MEMS Micro-ElectroMechanical Systems

MUX Multiplexer

PAM Polyacrylamide

PE Printed Electronics

PEDOT:PSS Poly(3,4-ethylenedioxythiophene):Polystyrene Sulfonate

PET Polyethylene Terephthalate
PH grip Paper with Hydrogel Grip
PV grip Paper with Velostat Grip

PVA Polyvinyl Alcohol

PVDF Polyvinylidene Fluoride

R_{bias} Bias Resistor

SEM Scanning Electron Microscope

SYMBOLS

V Voltage

 V_{out} Output Voltage of the Sensor

wt% Weight Percentage

Ø Diameter

MOTIVATION

Wearable sensors offer a user-friendly experience with a straightforward *plug and play* setup that does not require any complicated arrangement. Furthermore, these devices can acquire reliable data in diverse, challenging environmental conditions, which gives them an advantage among other traditional ways [1]. As a result, wearables have been one of the biggest fields of interest in the technologic world. While its concept is not new, with electronic watches dating back to the 1980s, these smart devices represent the next wave of market demand following smartphones[2], [3]. Since their launch, these devices have evolved from being heavy and inconvenient to more suitable, portable and lightweight, catering to the ever-growing needs of users [3], [4]. Remarkable progress has been achieved by the implementation of web connectivity options, advancements in energy management and the development of micro-electromechanical systems (MEMS), which have greatly enhanced their capabilities [5], [6].

Numerous wearables with distinctive functionalities have emerged, leading studies to classify them into six groups: entertainment, lifestyle, fitness devices, medical, industrial and gaming [1], [3], [3], [5], [7]. This classification reflects the growing demand for wearable technology, urging many companies to strive for market share by developing and launching devices specifically targeted at high-demand areas like sports and healthcare [7]. Particularly in sports, these devices enable athletes and coaches to track and monitor their performance in real time. This capability allows for more efficient and precise performance optimization, offering a viable alternative to conventional methods. Existing literature has developed sensor systems for various sports, including tennis, where accelerometers and gyroscopes track parameters such as player location and ball speed. However, metrics like grip strength and handprint, both crucial in racket sports, are often overlooked. In the case of padel, a similar sport to tennis, there is a notable gap in research on wearable technology. Therefore, to overcome this deficiency, it is necessary to develop sensor systems that can measure data on hand position and grip strength.

The purpose of this master's thesis is to investigate the use of sustainable materials for the fabrication of a smart grip, designed to be seamlessly integrated into the handles of padel and tennis rackets. This device is intended to collect relevant data, such as hand pressure and handprint patterns, with the goal of helping players improve their performance and optimize their gameplay. Due to its flexibility and interesting piezoresistive properties, Velostat was investigated as the active material in two prototypes of the smart grip. Additionally, hydrogel droplets were also explored as the active material for a third prototype. To ensure sustainability of the smart grip, paper and cork were studied as substrates for the silver electrodes. Each prototype was tested to identify the most effective solution for this application.

This work is structured into four chapters: the first chapter provides background information and theoretical concepts necessary to understand this thesis, along with a review of the relevant literature in this field. The second chapter details the materials used and methods performed, including the fabrication of the three grips, the chemical characterization of Velostat and the mechanical characterization of all prototypes. Finally, the last chapter presents the conclusions of this study, along with future perspectives for research.

1 Introduction

Over the past few years, the rapid evolution of the Internet of Things (IoT) has given rise to the development of compact electronic devices that can be integrated into an individual's body. Known as smart wearables or wearable technology, these devices allow users to access information from anywhere at any time, making them key players in IoT [2], [3].

Smart wearables are equipped with wireless sensors that can be seamlessly incorporated into accessories or clothing, offering a comfort and lightweight design [3]. Their primary function is to sense and measure specific quantities, producing a mechanical, electrical or other types of output signal [2], [5]. Equipped with micro sensors, wearables are able to non-invasively monitor various personal data, such as heart rate, brainwave activity, movements, locations and several more [2], [3], [8]. Following data collection, an energy-efficient microprocessor processes the information by typically discarding raw sensing data. The refined data is then stored and transmitted to remote devices, such as mobile phones, through low-power wireless interfaces [2].

Wearables are used in various fields, including entertainment, healthcare, and sports and can come in a variety of forms, including armbands (FitBit), wristbands or sport watches (Polar sport watch), chest straps (Zephyr BioHarness^T chest strap), clip-ons for clothing or footwear (Nike+ iPod sensor) [1], [2], [5], [6]. Nikenjad *et al.* provided a comprehensive overview of smart wearables in their review of the state of the art. In their paper, they summarized these devices that have been explored across different industries, including healthcare, education, the military and others [3]. This studied revealed the vast realm of smart wearables and its applications, becoming increasingly popular in different day-to-day domains in a user's life [3], [7].

1.1 Wearables in sports

Sports and fitness activities aim to enhance physical fitness and various attributes, such as strength, speed, and agility, as well as fostering specific embodied knowledge and skills [7], [9]. For professional athletes, even a minor improvement in their performance can serve as a crucial distinguishing factor among other players [4]. Hence, a keen understating of a player's movement is one of many essential parameters to identify shortcomings and improve technique [10]. Therefore, performance analysis in sports involves the evaluation of players' techniques, strengths, and weaknesses during games to gain insights not only to enhance their performance and achieve their desired goals but also to aid in injury recovery [4], [11].

Traditionally, performance analysts capture training and game sessions, producing video highlights to facilitate the players and coaches performance assessment. This method utilizes video sensors for tracking athletes' movements, yet it holds limitations such as inflexibility, lack of real-time data extraction and time-consuming post-processing. Therefore, creating a complete and comprehensive profile of a player's performance requires a setup of multiple synchronized cameras, making this system exclusive and expensive [4], [12].

The limitations associated with video-based analysis methods demand for alternative tools that can offer quicker, real-time solutions for sports performance analysis [4], [9]. Wearable technology designed for sports and fitness has gained significant popularity, particularly within the realms of personal tracking devices and sport watches, by presenting them as a viable alternative to conventional methods [4], [9]. Recent advances in sensor technology, coupled with a substantial decrease in the cost

of wearable devices, have enabled professional and amateur athletes to meticulously track and analyse their performances, without any discomfort, to ultimately optimize their results [4], [9], [13], [14]. These devices are set apart from other portable gadgets like smartphones due to their seamless integration into daily life, allowing them to operate discreetly [11].

Sports wearables encompass items such as sports watches, wristbands, heart rate monitors and sports equipment like rackets [11], [15]. Rana *et al.* compiled a review of commercially available wearable sensors for sports analytics which include Zepp Tennis 2, a wearable mounted on a tennis racket that measures racket speed, potential ball speed and others; Kinexon Perform, a wearable that could be clipped on t-shirts or trousers that monitors acceleration, change in direction, max speed and others [4].

The effectiveness of the wearables' analysis is dependent on the placement of sensors within the equipment, whether they function as accessories or not [6], [16], [17]. Büthe *et al.* presented an innovative wearable system that timed footsteps and arm gestures of a tennis player simultaneously. The authors explained that placing a wearable in both the player's shoes and the racket provided insight data on the timing of the player's footwork and racket swing. This "physical awareness" helped players achieve a successful shot [1]. In a study by Yamashita *et al.*, the researchers developed a smart table tennis racket with piezoelectric sensors to determine ball impact localization and stroke classification. The study successfully demonstrated that variations in output voltage could identify different shot types and impact locations, suggesting that this wearable could be valuable for training and gameplay [14]. These studies, along with many other, corroborate that sensor location remains a critical design consideration, with the main focus being on achieving the intended functionality [6], [12].

1.2 Wearables in Tennis and Padel

Focusing on the theme of this thesis, this chapter provides an in-depth analysis of wearable technology in tennis and padel. Tennis, a classic sport with a vast history and prestigious tournaments, is a technique and strength orientated game that requires a balance between aerobic and anaerobic endurance, explosive strength, power, and agility [4], [10]. Padel, while similar in its technical demands, has only experienced a significant rise in popularity over the past decade, leaving the academic literature limited. Both sports are extremely important nowadays, making this study valuable and noteworthy, not only for enriching the state of the art on padel but also for continuing to inspire curiosity and prestige in both sports.

Sensors like accelerometers, gyroscopes, thermistors and pressure sensors are heavily used in wearables for tennis [4], [1], [10], [18]. Connaghan *et al.* developed a sensing platform to provide both contextual and physiological feedback to the coaches and players. The goal of this study was to offer synchronised sensing of the player – such as heart rate and respiration through wearable sensing technology - and the environment, including the player's location and their movement over time, using custom-built sensing infrastructure. These parameters were captured by cameras strategically placed around the court, and a thermistor and an accelerometer positioned in the shirt [10]. In a 2019 study by Zhao *et al.*, a tennis assistant system was presented, composed of a motion sensor attached to a tennis racket to obtain data during gameplay. This system was able to extract ball speed and stroke data, achieving a 10.8% improvement compared to the state of the art [18]. Ebner *et al.* conducted a study examining the optimal position for the inertial measurement unit (IMU) sensor – either the wrist or the racket- to improve stroke detection and classification. Their findings revealed that the sensor provided equally accurate results regardless of whether it was placed on the wrist or the racket. Despite this underwhelming result, this study closed a gap in the state of the art by comparing the position of the sensor [19].

As shown in the examples above, these devices, often placed on different body parts and the racket, are not seamless for the player. In addition, commercial products that measure external workload, such as shot count, still need further development due to issues like limited accuracy and motion classification problems [19], [20]. Moreover, as mentioned before, padel has only gained a lot of international presence in recent years - therefore the state of the art is still limited. Most of the existing

studies on padel focus on anthropometric data and match analysis to determine performance outcome measures, *e.g.*, the age and gender, effectiveness at the net, serve and serve-return strategies, length of the rally and shot efficacy [21], [23], [24].

Hence, this work proposes to develop an innovative smart grip for padel and tennis rackets with cutting-edge technology to gather gameplay data such as grip strength and hand position, allowing athletes to assess performance and, ultimately, helping them improve their game. This smart grip is based on flexible pressure sensors, and, to the best of our knowledge, no similar technology currently exists in these sports. As a result, the smart grip can be considered a pioneering advance, as shown in Figure 1.1. While there is substantial research on flexible pressure sensor arrays, their application in sports rackets is scarce, typically limited to position maps or presence monitoring [25], [26]. One notable exception is the work by Yamashita *et al.*, who developed a sensor for ball localization and stroke classification using an array of ultrathin piezoelectric sensors. Their study proved that this sensor could successfully estimate the impact position and classify different strokes, but it was limited to table tennis rackets [14]. Other studies present similar wearables incorporated in table tennis [13], [15], [27], however none of them made the transition to tennis or padel.

In this work, materials such as Velostat, a flexible piezoresistive compound, coupled with silver tracks screen printed in paper and cork, as well as a paper sensor, featuring hydrogel droplets embedded beneath a printed silver matrix, will be explored for the smart grip. With that, the smart grip along with its materials will be discussed further in this report.

The proposed sensor system aims to revolutionize training and game analysis in tennis and padel as well as wearable sensors in sports. By collecting and evaluating key data point, players and coaches can gain deeper insights into performance and optimize their training strategies. Additionally, the use of a smart grip with IoT technologies opens the door for a more competitive gaming experience and the opportunity to increase the involvement of the player.

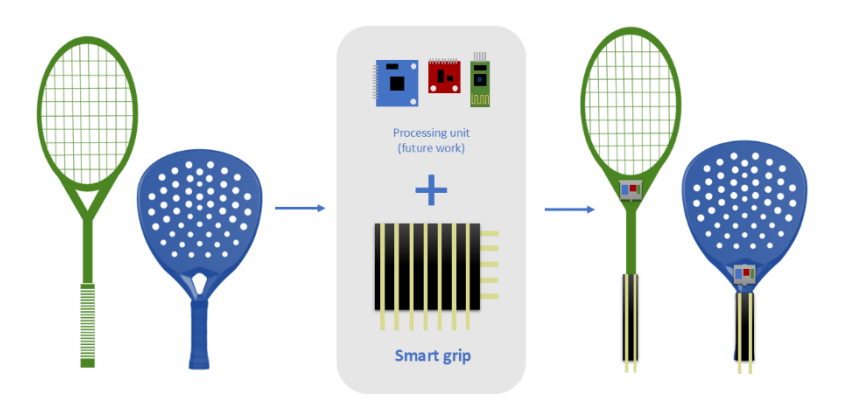


Figure 1.1 - Schematic of the smart grip application on tennis and padel rackets.

1.3 Smart grip

As mentioned before, the smart grip will be the keystone of the proposed sensor system. Its purpose is primarily to measure grip strength and recognize hand position. Therefore, the choice of the materials' grip must take in consideration certain characteristics such as pressure sensing, flexibility, mechanical and structural strength. Additionally, since the material is going to be in contact with the player's hand, it needs to be lightweight, and seamless to not hinder the player's performance. Moreover, the smart grip will be prone to wear due to the pressure applied by the player, thus its material must be able to withstand aggressive handling, making it crucial for the grip to be both robust and sturdy.

Therefore, opting for a sustainable, or recyclable material could be an advantage, considering its wear and tear.

Pressure sensing devices encompass piezoresistive, piezoelectric and capacitive methods [28], [29]. Piezoresistivity refers to changes in the electrical resistivity of semiconductors or metals when subjected to mechanical strain [29], [30]. This mechanism constitutes one of the four types of flexible resistive sensors designed for force sensing, each categorized according to distinct underlying physical phenomena. Another type is the strain gauge, which works by detecting resistivity changes when a conductor deforms. Aside from these, there is also quantum tunnelling that occurs in composite materials composed of conductive particles scattered within a polymer matrix. The final category is percolation, where materials transition from insulators to conductors [29], [30], [31].

Low manufacturing cost, flexibility, noise-resistant, the adjustability of the sensor's measurement range to accommodate specific loads, simplicity of interfacing circuits and data acquisition process represent the main advantages of these devices [31]–[36]. Resistive-based systems can be achieved with semiconductive pressure-sensitive inks or polymer-conductor composites like Velostat [30]–[32]. These devices can be employed in applications like wearable sensors and human-machine interaction devices [31]. However, the application of piezoresistive sensors is constrained by the aging of their materials, causing alterations in their electrical properties. With that, piezoresistive materials deform over time, preventing them from fully returning to their initial state. Additionally, these sensors often require calibration due to issues like from nonlinearity and significant hysteresis. They are temperature and humidity dependent, making them susceptible to environment changes [29], [31]. While these factors may affect their accuracy and repeatability, careful management and calibration can help mitigate these limitations. [31].

The innovative smart grip can be viewed as a tactile or touch sensor, as it responds to mechanical interactions with the player's hand [37][38]. In turn, polymer-based materials and composites are very promising in these types of sensors due to their stability, versatile properties, and stimuli-dependent electrical conductivity [31]. Along with these materials, tactile sensors demand efficient and precise systems for transducing analytical signals like an analog-to-digital converter or, often, simply called ADC [31]. These processing units are typically integrated in a microcontroller such Arduino and Esp32 [39]. These devices are able to convert input signal, such as voltage, into a quantified value and calculate the desired output signal, for example, resistance [25]. This type of technology has witnessed a major research effort in developing new materials and transduction mechanisms [37].

1.3.1 Velostat

Velostat, also known as Linqstat is a composite polymer material consisting of carbon impregnated polyethylene which, due to its properties, is one of the most stable and reliable material for tactile sensors [30].

Since the Velostat is entrapped with carbon black powder, quantum tunnelling or percolation properties are excepted [30], [31], [40]. As stated before, quantum tunnelling takes advantage of the conductive nanoparticles scattered inside the material's matrix. The tunnel effect is caused by applied pressure which deforms the polymeric material and changes the distance between particles, allowing the Velostat to alter its conductivity [31]. Even without physical contact, particles can still exhibit the tunnel effect through electrical interactions. Moreover, percolation properties create direct conductive routes inside the Velostat as a result of changes in the contact area of conductive particles brought on by material deformation, consequently affecting its conductance [31]. These characteristics enable the polymer composite to interchange from a dielectric polyethylene to an electrically conducting composite material [30], [31]. Therefore, when no pressure is applied, the Velostat is completely electrically resistive [25]. In a static measurement, where a specific weight is loaded onto the Velostat, higher loads increase conductivity and, consequently, lower resistance as the path of electrons shortens. The abovementioned physical phenomena defines the Velostat's electrical resistance and, therefore, sensitivity [31].

Velostat is a promising alternative material for this application, due to properties like flexible range of dimensions, low cost, mechanical and chemical stability [30], [31]. Li *et al.* utilized the amazing properties of Velostat to create a low-cost mat for step pressure and position mapping. Their mat not only was capable of effectively detecting the pressure change from a participant's step but also show the precise location of the step [25]. Similarly, Dzedzickis *et al.* studied the characteristics of Velostat by implementing it into a flexible tactile sensor [31]. Both studies highlight the promising potential of the piezoresistive material for force sensors due to its affordability, flexibility and suitability [25], [31]. However, some studies show that the performance of the Velostat concerning linearity, hysteresis and repeatability vary based on application and its environment. Thus, a review per application is essential [31], [32].

1.3.2 Cellulose-based substrates

Mechanical characteristics, composition, and structure of the electrode's materials significantly influence the overall performance of a sensor. Hence, developing new materials specifically tailored for piezoresistive measurements has significant importance [41]. Printing electronic (PE) technologies, such as screen-printing, inkjet printing and flexoprinting, emerged as a key method to manufacture and develop new materials for producing flexible sensors [28], [42]. The key advantages of PE technologies when compared with traditional silicon-based technologies, lies in its additive approach which leads to reduced material usage, faster fabrication processes, large-area deposition and, ultimately, a costeffective production [28], [42]. Moreover, these techniques offer benefits such as low manufacturing temperatures and the production of lightweight, flexible and conductive patterns of various shapes and sizes [28], [42], [43]. Emamian et al. proposed to use silver (Ag) flake ink as electrodes and polyvinylidene fluoride (PVDF) printed on polyethylene terephthalate (PET) to create a piezoelectric based touch sensor, demonstrating the great advantages of screen-printing [28]. Moreover, a study by Santhiago et al. on flexible cellulose-based devices for monitoring physical parameters demonstrates the effectiveness of screen-printing Ag conductive ink on paper as electrodes. This study found that this method enabled high conductivity and excellent mechanical stability in cellulose-based devices, making them highly suitable for wearables applications [40].

In the production of flexible sensors, the substrate plays a significant role in determining the overall flexibility and performance of the device. Typically, plastic serves as the conventional option for such applications. However, cellulose-based substrates like paper and cork are very promising due to their environment-friendly nature [44]. Notably, paper stands out not only as a sustainable material but also for its temperature resistance and rich wavy surface at microscale [28], [35]. The use of paper enables the sensor to conformably adapt to any type of surfaces, overcoming limitations in spacing and shape that would prohibit the use of a rigid conventional sensor [28], [35]. In turn, cork is a lightweight natural material with extraordinary properties, such as compressibility, impermeability and durability [44]–[48]. Moreover, cork is able to endure large deformations, followed by a fast recovery when stress is released. This characteristic is crucial in a pressure sensor since it ensures a low recovery time and sensor's longevity [48]. Therefore, these two materials have become of upmost importance in flexible sensing applications [28], [45].

1.3.3 Hydrogels as an active layer

To enhance the sensitivity of sensors, hydrogel droplets can be introduced between the parallel plates [41], [38]. Hydrogels are cross-linked 3D network polymers with a high percentage of water[41], [49]–[51]. Hydrogels contain large amounts of water, ions can easily be dissolved in them, rendering them ionic conductors [51]. Moreover, hydrogels have remarkable properties, including outstanding elasticity, stretchability, compliance, recyclability and, in certain cases, self-healing capabilities and reversible adhesion [41], [51]. As a result, pressure sensors, created by sandwiching hydrogels in between two conductor layers, have been gaining attention for the development of flexible sensors [41], [49]–[51]. Furthermore, the hierarchically wrinkled microarchitectures and interconnected ridges on the

hydrogel can substantially increase the contact area. Consequently, the hydrogel-based pressure sensor presents high sensitivity and precise sensing capabilities, particularly in capturing dynamic pressures [50].

Hydrogels can have different formulations depending on its constituents. Hoang *et al.* created piezoresistive tactile sensor with Poly(3,4-ethylenedioxythiophene):polystyrene sulfonate (PEDOT:PSS) with Polyacrylamide (PAM) hydrogels [52]. Moreover, Alemán *et al.* produced a conductive and self-healable hydrogel by mixing PEDOT with alginic acid applied in a highly sensitive pressure array [53]. Other authors opted to study cellulose-based hydrogels in pressure sensors, such as, Li *et al.*, who prepared a cellulose nanofibrils, carboxymethyl chitosan (CMC), polyvinyl alcohol (PVA) and lignin-based carbon (LC) hydrogel [36]; Chen *et al.* integrated sodium carboxymethyl cellulose (Na CMC) into polyacrylic acid doped with Fe³⁺ to fabricate high-strength and self-healing hydrogels [54]. These pressure sensors demonstrated great performances, offering promising new options for flexible wearable electronics.

After reviewing the state of the art, this work implemented an innovative hydrogel formulation, composed of sodium carboxymethyl cellulose (Na-CMC), calcium chloride (CaCl₂) and zinc chloride (ZnCl₂). This combination was selected based on its outstanding results in studies with similar applications conducted by AlmaScience. Due to their unique properties these hydrogels show great potential as an ideal material for the active layer in various pressure-sensing applications.

As mentioned above, in this work, three smart grips were fabricated from different materials to study their performance across various tests. These sensors were designed to measure specific data, such as grip strength, providing valuable feedback to the players, potentially transforming training and gameplay.

MATERIALS AND METHODS

This chapter provides an overview of the production process for three smart grips made from different materials, as well as their characterization to evaluate their behaviour and performance.

2.1 Production of the smart grips

In this study three smart grips were manufactured: paper with Velostat, cork with Velostat and paper with hydrogel. The sensors were designed in an 8 x 6 multi-layer matrix structure, featuring orthogonal electrodes on the top and bottom layers, with a pressure-sensing layer in the middle. A pixel is the active area of the sensor created by overlapping the electrode layers with the pressure-sensing layer sandwiched between them. Hence, each grip has 48 individual pressure-sensing pixels. Annex A.1 displays a schematic of grip prototypes.

The smart grip was divided into two parts due to slightly widening of the racket's handle at the bottom. Therefore, the upper part was dedicated to the octagonal prism, whereas the lower part was allocated to the trapezoidal prism. For a visual representation of these two parts please consult Annex A.2.

2.1.1 Paper with Velostat Grip

The top and bottom electrodes were screen-printed on a multi-function office paper (80 g/m² grammage, from The Navigator Company) using Saralon Saral SilverH2O 600 electrically conductive ink with a curing step of 120 °C for 10 min on a hot plate. Subsequently, the paper was cut into 12.5 x 0.5 cm² strips to form rows and 13.5 x 0.5 cm² strips to produce the columns of the matrix. To facilitate the connection of the strips to the cables in the breadboard, conductive thread (DFROBOT FIT0746, Sewing Thread Conductive Stainless Steel, 9 Ω , \emptyset = 0.42 mm) was employed via conductive connectors to ensure a seamless integration with the player. Heat-shrinking tubes from Gocableties, with 1.2 mm in diameter, were wrapped around the conductive thread and then shrunk using a hot air gun at 250 °C to prevent short circuit between different rows and columns. Additionally, the cables connecting the conductive thread to the breadboard were soldered with a loop at one end to enable knotting. These cables were connected to a readout circuit afterwards.

For the sensor active layer, a $11 \times 8.5 \text{ cm}^2$ Velostat sheet from Adafruit was used for the upper part of the grip. Moreover, in the lower part, the Velostat was cut into a $13 \times 3 \text{ cm}^2$ oval-shaped trapezium to ensure the proper fitting of the grip on the handle.

2.1.2 Cork with Velostat Grip

Similarly to the previous grip, the top and bottom electrode were screen-printed on an extremely thin sheet of agglomerated cork bonded over cloth substrate (from Verde Lima) using Saralon Saral SilverH₂O 600 electrically conductive ink. The printed cork sheet was cured at 120 °C for 10 min on a

hot plate. Then again, it was cut into $13 \times 0.7 \text{ cm}^2$ strips to produce the rows and $14 \times 0.7 \text{ cm}^2$ strips to fabricate the columns. The conductive thread, heat-shrink tube, cable connections to the breadboard were conducted in the manner as the previous grip.

The dimension of the Velostat for the upper part of the handle was $12.5 \times 8 \text{ cm}^2$, whilst the lower part was cut into a $13 \times 3 \text{ cm}^2$ oval-shaped trapezium, consistent with the paper with Velostat grip.

2.1.3 Paper with hydrogel Grip

The paper with hydrogel grip was produced in a slightly different manner than the Velostat grips. A matrix mold of the grip was developed in Cricut Design Space to design the desired rows and columns in adhesive paper. This paper was then glued to a screen-printing mesh (mesh model 120 from I.C.M Graf., Lda.) to serve as a pattern for the matrix. The bottom layer of the grip was screen-printed using the mesh with Saralon Saral SilverH₂O 600 electrically conductive ink onto multi-function office paper (80 g/m² grammage, from The Navigator Company). A curing step for 10 min at 120 °C was employed thereafter.

The top electrode underwent a different approach, since the hydrogel droplets were going to be dispensed and dry on it. First, a pattern of a 11.5 x 8 cm² rectangular and a 13 x 3 cm² oval-shaped trapezium was created by overlapping the rows and columns of the desired matrix. By inverting this pattern, the matrix's pixels were made evident. For a visual understanding of this layer, please refer to Annex A.3. Using a wax printer, the pattern was printed on paper and cured for 10 min at 150 °C on a hot plate to diffuse the wax into the paper, thereby creating barriers for the hydrogel. This procedure ensures that the hydrogel droplets remain confined to the designated zones on the paper. After the curing step, the top layer paper was screen-printed in the same method as the bottom layer.

For the active sensor layer, a hydrogel solution consisting of 5 mL of 2.5 wt% sodium carboxymethyl cellulose (Na-CMC, CAS: 9004-32-4, Sigma-Aldrich, Mw ~250,000), 1 mL of calcium chloride dihydrate (CaCl₂·2H₂O, CAS:10035-04-8, Sigma Aldrich) and 1 mL of zinc chloride (ZnCl₂, CAS 7646-85-7, Sigma Aldrich) was used. The latter two having a concentration of 1 M. After, it was magnetically stirred for 5 min at room temperature until the solution turned white, which meant that the hydrogel had crosslinked. The hydrogel was dispensed onto the reverse side of the top layer on the designated zones with a 1 mL micropipette. Each pixel was covered with 30 μ L of hydrogel, resulting in a total usage used 1.44 mL for all 48 pixels (30 μ L x 48 pixels = 1440 μ L of hydrogel). The top layer was left to dry overnight.

Finally, to assemble the grip, both layers were aligned and glued together using double-sided tape. A small hole was punctured on the second section of the grip and concealed with silver ink to electrically connect both sections. More information can be found in Annex A.4.

2.2 Readout circuitry

The sensors matrix was controlled by a readout circuitry that integrated a microcontroller, a multiplexer (MUX), a demultiplexer (DEMUX), and a bias resistor (R_{bias}), The Esp32-Wroom-32U (Esp32) microcontroller was selected for this purpose due to its excellent performance and simplicity. M74HC4051 PDIP-16 models were chosen for both the MUX and DEMUX. Each grip was connected to a bias resistor creating a voltage divider circuit at each pixel. Consequently, the output voltage (V_{out}) is given by Equation (1)

$$V_{out} = \frac{R_{sensor}}{R_{sensor} + R_{bias}} \times V_{in} \tag{1}$$

where R_{sensor} is the resistance of the grip and V_{in} is the input voltage. With that, the Esp32 scans the values of each pixel by dynamically switching between rows and columns through the MUX and then quantifies the data using its built-in ADC. Next, the digital signal is processed through a program written in JavaScript and generated into a real-time picture for visual representation of the smart grip and the

player's hand. This seamless process ensures precise and reliable measurement across all grips. Annex A.5 shows a schematic diagram of the circuitry.

2.3 Characterization of the smart grips

Surface morphology images of the piezoresistive material, Velostat, were acquired using a Zeiss Supra Ultra-Performance Field Emission scanning electron microscope (SEM) Hitachi Regulus SU8220 (Tokyo, Japan). Chemical characterization of Velostat was performed by the SEM equipped with energy-dispersive X-ray spectroscopy (EDXS). Four dynamic pressure tests were carried out by a Shimadzu Tensile tester EZ-LX (Kyoto, Japan) equipped with a 5 cm cylindrical force gauge. The tests were defined by the displacement of the force gauge, referred to as the stroke, which corresponded to the distance the gauge travelled relative to the sensor under an applied force. For example, in the tests involving the cork with Velostat grip, to apply a force of 100 N the pressure machine was programmed to displace the force gauge approximately 1.4334 mm against the sensor. This displacement was calibrated individually for each applied force and each grip configuration.

The first test, "Steps", was performed by applying force to the grip in the following sequence: $0 \times 100 \times$

RESULTS AND DISCUSSION

This chapter focuses on the detailed characterization of three smart grips composed of different materials, providing comprehensive insights into their mechanical properties and performance. First, a more in-depth review of Velostat, a piezoresistive material used as an active component in two of the smart grips, is presented. Next, each smart grip and its corresponding characterization are showcased.

3.1 Velostat

Velostat is a polymer composite composed of polyethylene, a plastic substrate, and carbon black, a conductive filler. Its composition allows it to exhibit the tunnelling effect and percolation properties, explained previously in Section 1.3.1. Due to its low cost and commercial availability, Velostat has been widely used in applications such as touch sensors and pressure mats [30], [55]. To gain a deeper understanding of the Velostat properties and composition, SEM and EDS were applied for characterization.

3.1.1 Morphological Characterization

To evaluate the Velostat surface morphology, surface imaging of two samples from different producers was performed in SEM (Figure 3.2). Figure 3.1 presents the two characterized samples, both from Adafruit.

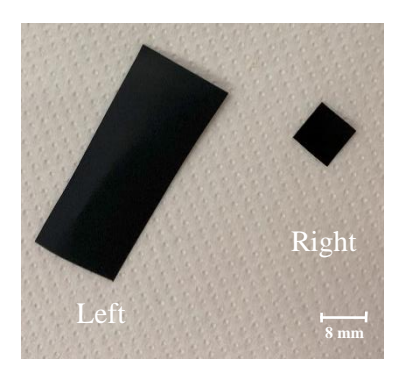
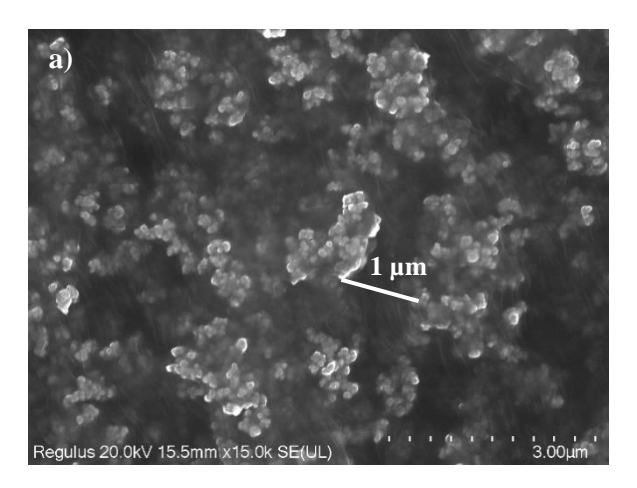


Figure 3.1 - Samples of Velostat from Adafruit.

Both samples were observed in SEM under 15 000x magnification. The white clusters represent carbon particles, whereas the black background indicate the polymer substrate. However, in Figure 3.2 it is possible to note the main differences between samples. Figure 3.2 a) appears to contain a higher

amount of carbon compared to Figure 3.2 b), as evidenced by predominant white spots in sample a). This difference can be even seen with the naked eye since the left sample from Figure 3.1 is hazier than the right sample. Under normal conditions, without any pressure applied, the polymer clusters average a distance of 1 μ m. At this distance, the resulting electric current is at the picoampere range, making the Velostat highly electrically resistive. Preliminary experiments were conducted using a UNI-T UT890C multimeter to measure the Velostat's resistance under no pressure. However, it was observed that no measurable resistance was detected, suggesting that the resistance exceeded the multimeter's upper limit of 60 M Ω . When pressure is applied, the distance between clusters is reduced to around 0.6 μ m. This compression facilitates the formation of direct conductive pathways within the Velostat sheet, allowing it to start to conduct electricity [25], [56].



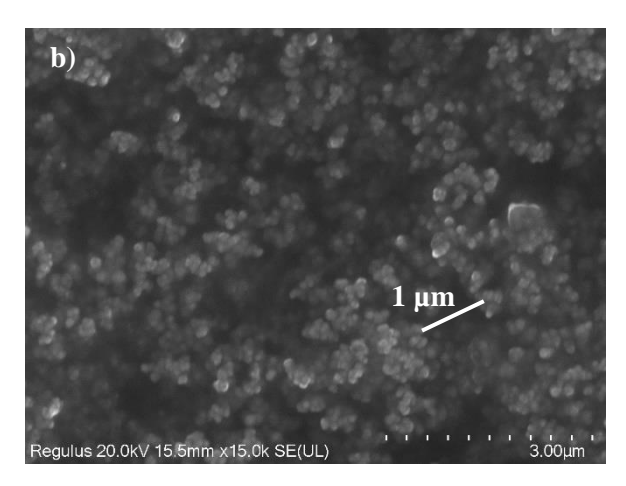


Figure 3.2 - SEM visualization of Velostat samples displayed in Figure 3.1: a) left sample; b) right sample.

The EDS method was also employed to perform quantitative elemental analysis to both samples. Elemental mapping was conducted during the EDS analysis as show Figure 3.3.

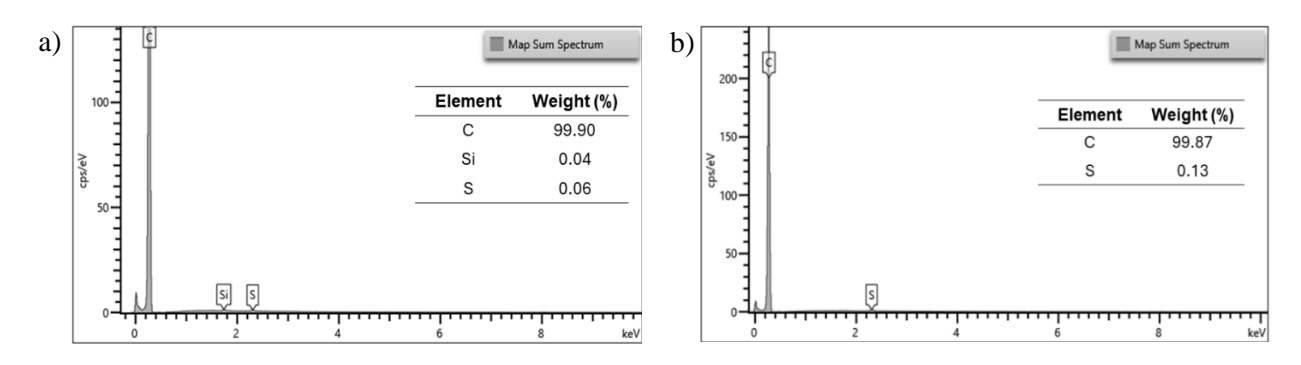


Figure 3.3 - EDS Spectra of Velostat samples displayed in Figure 3.1: a) left sample; b) right sample.

The EDS spectrum depicts a dominant peak at around 0.3 keV corresponding to carbon (C), with a 99.90 wt% in Figure 3.3 a) and 99.87 wt% in Figure 3.3 b). This confirms that the Velostat is predominantly composed of C as mentioned before. In Figure 3.3 a), two other minor peaks can be observed at 1.7 keV, corresponding to silicon (Si) with 0.04 wt%, and at 2.3 keV, corresponding to sulphur (S) with 0.06 wt%. Figure 3.3 b) indicates only one other minor peak at 2.3 keV that demonstrates the presence of S with 0.13 wt%. Velostat is made with carbon black and polyethylene, thus neither S nor Si are included in its composition. Therefore, the peaks associated with Si and S can be attributed to contamination that occurred either during the handling the sample or the production

process. Despite slight variations in the composition of both samples, the performance of the two Velostat sheets showed no significant differences when tested with a simple voltage divider.

3.2 Smart Grips

In this section, three different grips will be studied and analysed in detail. Table 3.1 summarizes the structure of these grips, which will be discussed in detail in the following sections.

Table 3.1 – Overview of the structure of the smart grips studied in this work

GRIPS	STRUCTURE (Crossbar)	SUBSTRATE (Screen-printed with Ag ink)	ACTIVE MATERIAL (Piezoresistive)	
Paper with Velostat	6.0	Paper	Velostat	
Cork with Velostat		Cork	Velostat	
Paper with hydrogel		Paper	Hydrogel droplets	

All grips were connected to same readout circuitry, as explained in Section 2.2. However, different R_{bias} were connected to different grips due to their varying internal resistance. The grips were characterized by obtaining the voltage variation when varying forces through a tensile tester equipped with a force gauge. After reviewing numerous studies on grip strength across various demographics, it was concluded that the forces most similar to those exerted by athletes were 100 N, 250 N, 350 N and 500 N [23], [24], [57]–[60]. These studies included participants of different ages, genders and levels of padel and tennis experience, providing a comprehensive and vast insight into how grip strength varies [23], [24], [57]–[60].

Four tests were planned to investigate the performance of the sensor as well as its durability. In a padel or tennis match, male professional players can exert up to 50 kg of force in grip strength, while female high-level players apply a force of approximately 30 kg [23], [24], [57]–[60]. Therefore, the smart grip must withstand these pressures daily. Furthermore, durability is a crucial aspect of a smart grip for rackets, as they must endure these significant forces applied by the player's hand. Both padel and tennis involve various strokes, such as, volleys, forehand, backhand, smash and many others [23], [58]. These movements require different handling of the racket and, hence, applied force. Thus, the smart grip must have the ability to differentiate between a wide range of pressures. Accordingly, the

pressure tests were designed to assess various movements and their corresponding forces. The first test, 'Steps', was designed to recreate a simple chain of actions that could occur during a game: first, a volley applying 100 N of force, then a forehand requiring a bit more force (250 N) and finally, a smash, which requires much greater force (500 N). The second test, 'Continuous Pressure' aimed to study the responsiveness to moderate force (350 N) over a prolonged period of time, as well as the recovery of the output signal. Finally, the tests 'Cycles 0 to 100 N' and 'Cycles 0 to 500 N' were used to simulate the game's speed, as there is nearly an action per second during gameplay [21], [23], [60]. The tests' results are presented in the next subsection.

3.2.1 Paper with Velostat Grip (PV grip)

Figure 3.4 a) illustrates the PV grip, in which is visible 4 lines and 4 columns made with Ag ink screen-printed on paper with Velostat in between. Initially, a simpler 4×4 matrix was created, instead of an 8×6 , to become familiar with the testing process using the pressure test machine. Additionally, since this was the first attempt, a smaller matrix was chosen to minimize waste in case the testing did not go as planned. The paper strips were cut to same size width in both matrices, guaranteeing the same size pixels, $0.5 \times 0.5 \text{ cm}^2$. The pixel pitch was around 0.5 cm. Figure 3.4 b) demonstrates the 8×6 grip applied to a padel racket.

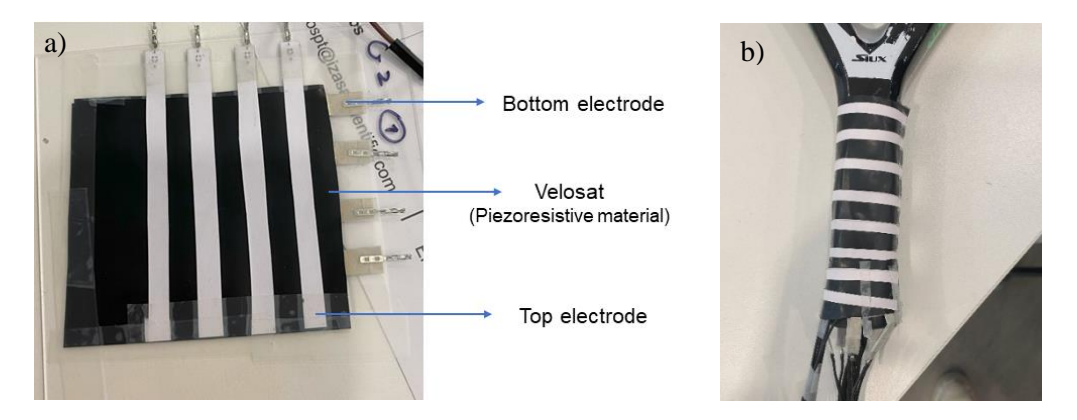


Figure 3.4 - Paper with Velostat grip: a) structure; b) grip mounted on the racket.

3.2.1.1 Pressure Machine Tests

Figure 3.5 illustrates the setup with the tensile tester equipped with a force gauge with a diameter of 5 cm as well as a schematic of the placement of the force gauge. It is possible to see that the force gauge did not encompass the whole sensor, hence, the 4 pixels on the extremities of the sensor were not pressed.

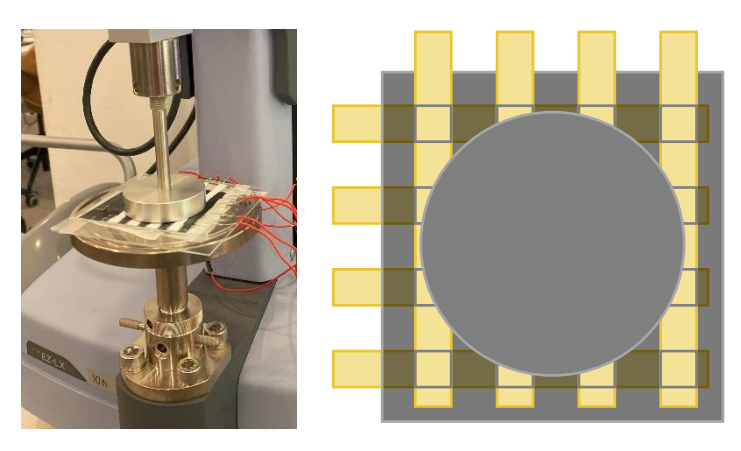


Figure 3.5 - Pressure machine setup and schematic for testing of the paper with Velostat grip.

3.2.1.1.1 Steps

Figure 3.6 shows the response of the PV grip along with a color-coded sensing map of the grip's pixels which provides a detailed understating of how the force was distributed and sensed across the array. The results are shown for two cases: with $R_{bias}=1~k\Omega$ (Figure 3.6 a)) and with $R_{bias}=330~\Omega$ (Figure 3.6 b)). The colours in both graphs and sensing maps represent varying response levels: blue indicating low responses, green representing moderate responses, and red showing stronger responses.

Similar sensors from published studies suggested different R_{bias} , ranging from 550 Ω to 2.2 k Ω when using Velostat as a piezoresistive sensing element [25], [61]. With that, two resistors (1 k Ω and 330 Ω) were tested as the R_{bias} component within the readout circuitry to determine the most suitable option. The following test was designed to mimic a simple sequence of strokes in padel/tennis, initiating with a volley, around 100 N, then a forehand, 250 N, and finalizing with a smash, 500 N.

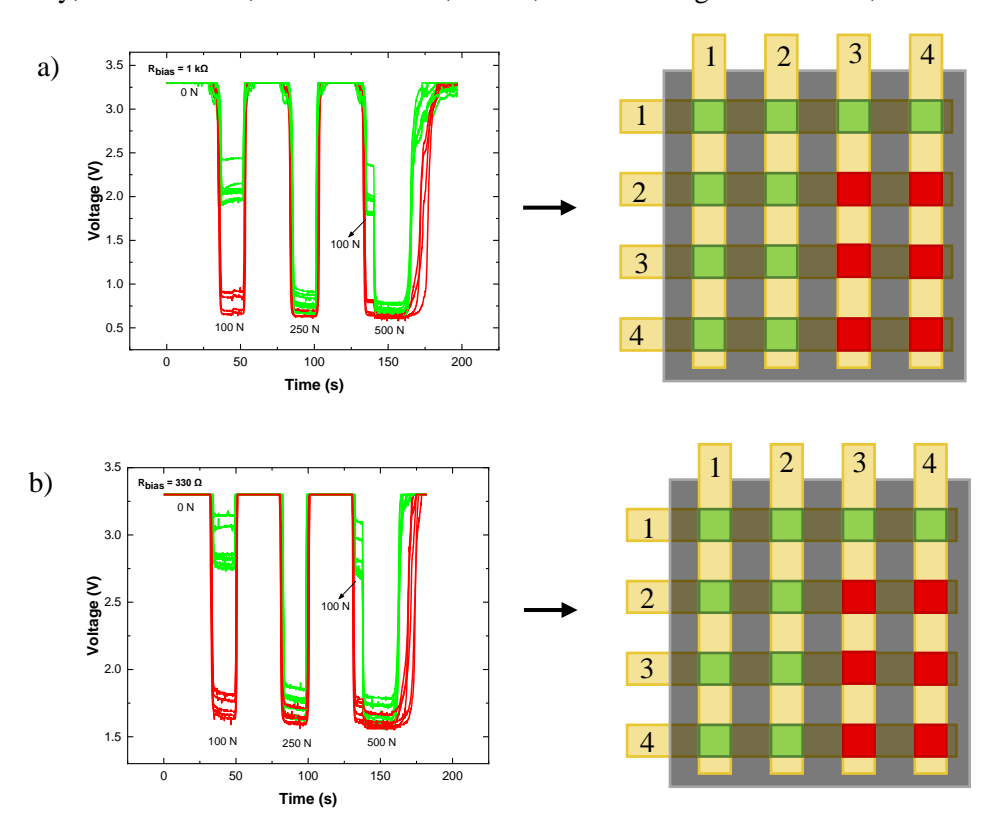


Figure 3.6 -Performance of the smart grip during the Steps test: a) using a Rbias = $1 \text{ k}\Omega$; b) using a Rbias = 330Ω .

The first attempt of testing this grip was made as illustrated in Figure 3.6 a). For each step, the sensor's response was almost identical, as it could not clearly differentiate between high and low forces, especially for forces higher than 250 N. This resulted in a consistent voltage drop of 2.8 V for the red traces. The green traces showed a 1.3 V drop for the 100 N step, however in the second and third step, the sensor could not differentiate between different forces, demonstrating a voltage drop of approximately 2.8 V. Despite this, the smart grip responded quickly to the stimulus of the pressure machine for each step. In the last step, the recovery time was slower and varied among pixels. This could be attributed to the high force of this step, combined with the sensor not being completely flat. As a result, the force gauge may have contacted different pixels in varying ways, leading to different sensing from each pixel. Additionally, the extremities of the sensor experienced crosstalk, *i.e*, a non-pressed pixel responds as if there was an object on them [56], [61]. This phenomenon was expected mainly due to the crossbar architecture of the electrode and continuous film of Velostat. Once the force gauge contacts with the grip, the carbon particles impregnated in the Velostat become closer together and start to electrically conduct even if they are not touching through a process called quantum tunnelling. [56], [61]. Hence, a pressed carbon particle can conduct current through neighbouring particles, leading to

random current flows through the entirety of Velostat film [56], [61]. The grip's performance meant that it struggled to distinguish between forces, likely due to the R_{bias} being too high, leading to large amounts of current to flow through the Velostat and, thus, resulting in overly high sensitivity. To counter this, a smaller R_{bias} was implemented on the readout circuit, ensuring a decreased current flow through the sensing element since current always flows through the path with smaller resistance. Figure 3.6 b) showed the sensor's response to the same test but with a R_{bias} of 330 Ω . Here, the grip responded similarly to the previous test, however with smaller voltage drops of around 1.7 V for the red traces. It is also visible that green traces had a significantly smaller drop, roughly 0.55 V, when compared to Figure 3.6 a). Furthermore, this sensor demonstrated quick recovery times, showing significant improvement in the last step with much faster recovery, though it still could not differentiate forces, especially above 250 N. Different sensing was still visible during the last step, especially in recovery, however it was much less than in the previous test. This grip also demonstrated crosstalk, nevertheless, it was significantly less than what was observed in Figure 3.6 a). Considering the slightly better grip's response in Figure 3.6 b), the $R_{bias} = 330 \ \Omega$ was selected as the load resistor for the subsequent tests.

3.2.1.1.2 Continuous Pressure

In Figure 3.7 a), the performance of the PV grip and the sensing map during the Continuous Pressure test are presented, where a force of 350 N was applied during 60 s, followed by 15 s rest and then reapplied for 180 s.

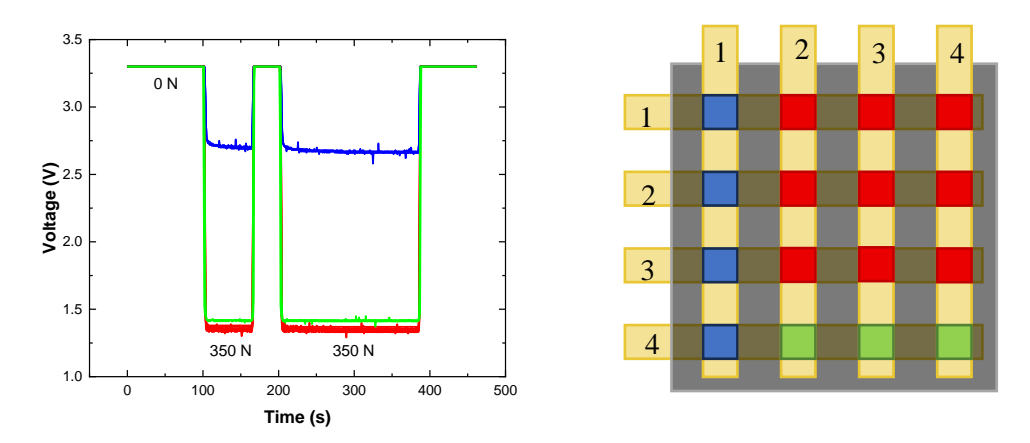
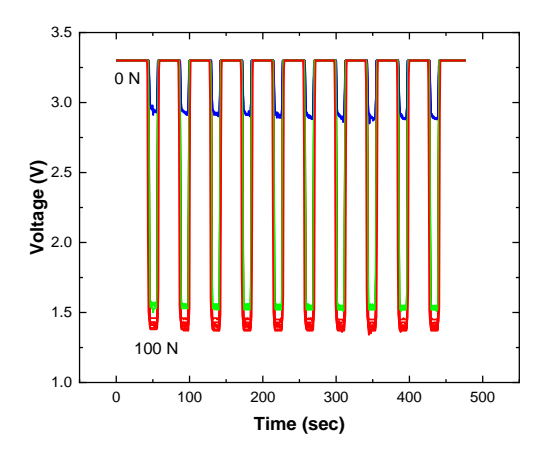


Figure 3.7 - Performance of the smart grip and the corresponding sensing map during the Continuous Pressure test.

The sensor had excellent response to this durability test, maintaining continuous response without any variations throughout the entire process. There are evident signs of crosstalk in the blue traces corresponding to column one, as it has a significantly less prominent drop, approximately 0.55 V, when compared with the other pixels. Since the force gauge was too small to cover the entirety of the sensor, leaving the extremities nearly untouched, random current must have flowed through the Velostat sheet, causing output signals to be detected in non-pressed pixels. The green and red trace show a significant voltage drop, roughly 2 V, indicating a substantial response to the force. Despite the varying levels of voltage drop due to crosstalk, all pixels responded simultaneously when the force was applied. This can be observed in Figure 3.7, where each sensor's voltage began to drop at around the 100 s mark, and, similarly, all sensors showed a voltage recovery at approximately 160 s. Despite not being a plausible scenario in a real-life game, Figure 3.7 displays how effectively the smart's grip response is to prolonged pressure. This indicates that the sensor is reliable over extended periods, which is valuable for this application.

3.2.1.1.3 Cycles 0 to 100 N

The grip was subjected to 10 cycles of force application, ranging from 0 to 100 N, as illustrated in Figure 3.8.



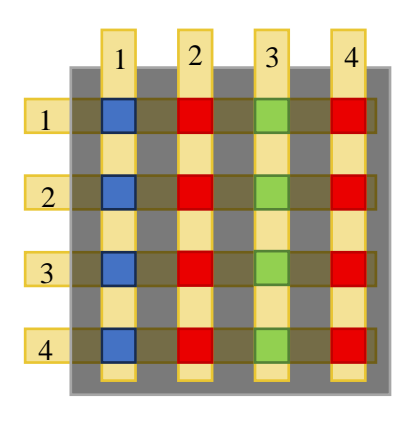


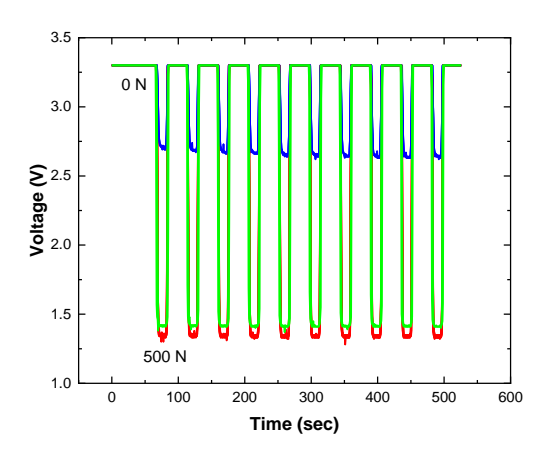
Figure 3.8 - Performance of the smart grip and the corresponding sensing map during the Cycle 0 to 100 N test.

The green traces, corresponding to column three in the schematic layout, presented a similar response to the red traces in the plot. The green traces had a voltage drop of about 1.8 V for the application of 100 N, while the red traces presented a voltage drop of 1.9 V. This grip is a flexible wearable, which means the Velostat sheet may shift slightly during each test and, in this case, cycle. As a result, the difference between the responses of the red and green traces may be attributed to the Velostat layer not being completely flat during this cycle test.

Moreover, by observing Figure 3.8, the blue traces (column one) dropped from 3.3 V to around 3 V in each cycle. With that and considering that the diameter of the force gauge was too small to encompass the sensor entirely, it is possible to conclude that column one suffered crosstalk. Nonetheless, the grip had a rapid response in each cycle, with both response and recovery times being extremely small, proving that for this application, where frequent and quick actions occur, this grip could be a suitable option.

3.2.1.1.4 Cycles 0 to 500 N

By analysing Figure 3.9, the grip's response is comparable to the previous test. The output voltage drop for the red and green traces was once more around 1.8 V for each cycle, meaning that the smart grip could not discriminate between rapid force cycles of 100 N and 500 N. In addition, the pixels from the overlaying of lines 1, 2 and 3 with columns 2, 3, and 4 displayed a significantly more evident response than the rest. This can be attributed to the higher pressure applied in those pixels since the force gauge was directly pressing on them. The main difference between the cycles tests was the crosstalk effect in column one. Here, the pixels from the first column of the matrix exhibit a higher level of this effect. The increased force applied in this test, 500 N, compared to the 100 N used in the previous test could explain this difference.



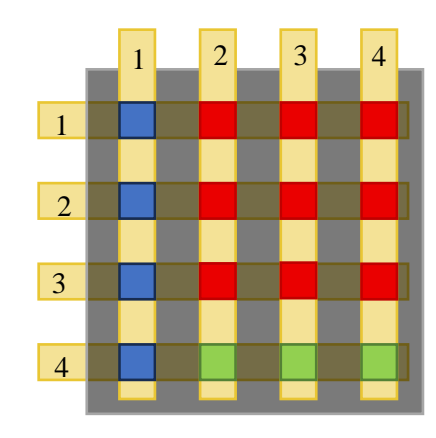


Figure 3.9 - Performance of the smart grip during the Cycle 0 to 500 N test.

3.2.1.2 Player-interface evaluation

After the grip's performance in mechanical tests, the grip was also studied under real-life conditions. Four subjects were selected to perform a series of tests to gain a deeper understanding of the sensor's performance. These subjects were selected to represent a spectrum ranging from individuals who had never played padel before to those who are professional players. The smart grip was mounted on a padel racket, as one was readily available. However, these results can easily be extrapolated for tennis players, given the similarities between the two sports. Table 3.2 represents the demographic of the selected volunteers.

Table 3.2 – Description of users and their experience level in padel for the player-interface test.

	PLAYERS	EXPERIENCE
1	Non-Player (NP)	None
2	Non-Player (NP)	Little
3	Player (P)	Recreational Player
4	Player (P)	Professional Player

These tests were analysed through a generated matrix of the smart grip done with a post-processing program. The received data is converted into an 8 x 6 matrix, corresponding to the sensor array of the smart grip for a proper visualization. The microcontroller scans the matrix every 0.1 s and the program converts and stacks together the real-time pressure data into a matrix.

In this experiment, the subjects were initially instructed to hold the racket without applying any force. At this stage, a picture of the generated matrix was taken to capture the sensor's response. Subsequently, the volunteers were asked to hold the racket with maximum force. Another picture of the grip's response was taken to be analysed further on. This test allows a comparative analysis of the matrix responses under different force conditions, providing insights not only of the performance of the grip during a real-life environment, but also its endurance to wear and tear. Figure 3.10 summarizes the results of the test. The matrix was designed to display to the pixels in different shades of green depending on the voltage chance, with a more pronounced voltage change resulting in a darker green hue, and viceversa.

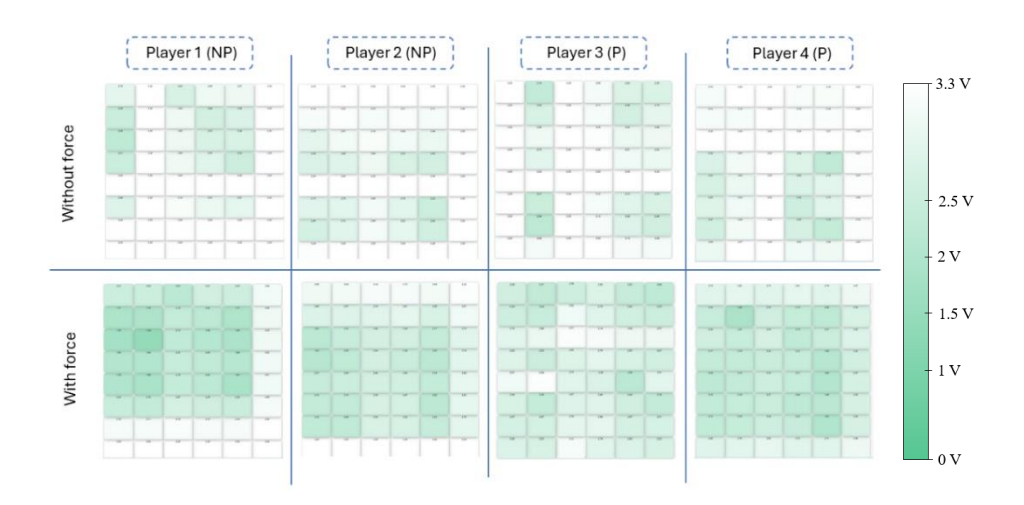


Figure 3.10 - Players performance with the paper with Velostat grip during player-interface evaluation.

Players 1 and 2 were the volunteers with less experience, hence a much higher placement of the hand on the grip was expected. While applying force, player 1 does not utilize the last rows and the last column, concentrating the pressure in the upper left part of the matrix. Each player has a unique way of holding the racket in a way that is more comfortable for them but, in this case, player's 1 way of holding the racket could be correlated with the lack of experience in racket sports. The same can be observed in the player's 2 results; however the matrix, where the maximum force was documented, has a more evenly distributed response than the player's 1 matrix. Player 3 displays a grip that differs from the others. While using the smart sensor as a whole, there are a few rows, such as row 3, where slightly less force is applied. This suggests that player 3 positions their index finger higher in the grip than the other players. In contrast, player 4, despite also utilizing the grip as whole, has a more pronounced grip at the bottom of the handle as seen in the picture with force applied. These differences highlight the distinct ways that players can grip the racket, demonstrating that this smart grip can effectively identify and analyse these variations.

During the pressure machine test, the PV grip maintained consistent output during the Continuous Pressure test and demonstrated impressive responsiveness and rapid recovery during the cycle tests. Nevertheless, this grip did not respond consistently to each force, meaning that the output voltage drop was similar for forces exceeding 250 N across all tests. This is not ideal, especially in this application due to the aim of the smart grip is to give detailed information of every stroke, thus the ability to clearly differentiate between various forces is a must. Additionally, the smart grip suffered considerable wear, particularly in the player-interface evaluation, due to extensive usage. For that reason, a screen-printed cork substrate with the same electrically ink was studied and discussed in the following section, in hopes of achieving improved results.

In Annex A.6 the grip after testing is displayed. The grip indicated significant signs of wear and tear, including torn paper strips and scratches of the screen-printed Ag ink, which results in poor electrical conduction and, in some cases, even complete loss of connectivity. While the Velostat remains largely intact, the paper strips have suffered the most damage. This indicates that the grip is not capable of withstanding continuous use. Since the application is intended for players to use during training, this grip does not present as the best solution for this purpose. One approach to improve the results is to cover the smart grip with a cloth-like overgrip, commercially available, ensuring its protection during training sessions. However, this option was not experimented, therefore further testing needs to be done.

3.2.2 Cork with Velostat Grip (CV grip)

The results of the prior grip were slightly underwhelming, so a new grip with different top and bottom electrodes was designed with the expectation of achieving better outcomes. A flexible cork

substrate was chosen as the electrodes' material for its robust structure and sustainability. This substrate was screen-printed with Ag lines and then cut to form both electrodes. In Figure 3.11, a schematic illustration of the sensor system as well as the racket equipped with the smart grip is shown.

Using the same readout circuitry with a 330 Ω R_{bias}, durability tests were conducted on the CV grip to study its performance and robustness. In the subsequent section, four mechanical tests – Steps; Continuous Pressure; Cycles 0-100 N; Cycles 0 – 500 N - are presented and analysed.

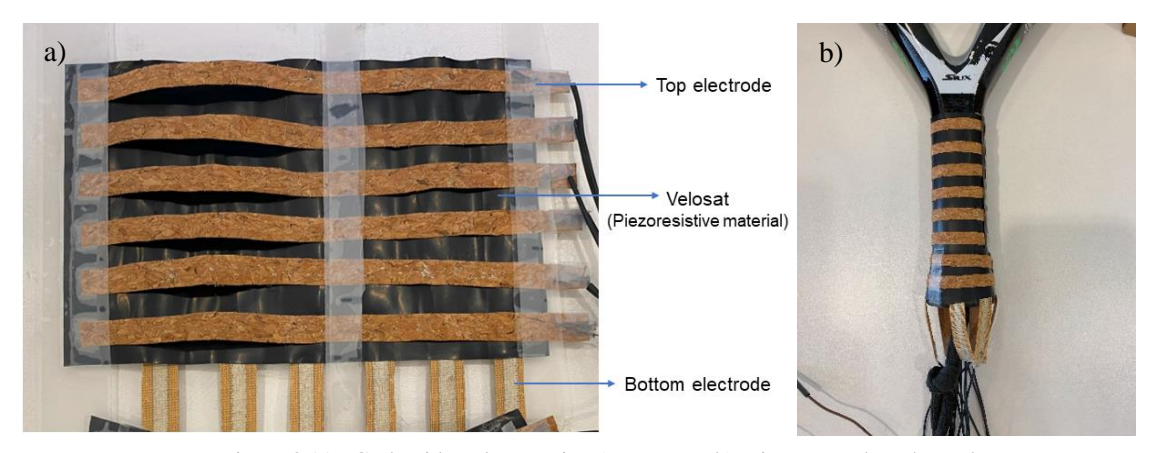
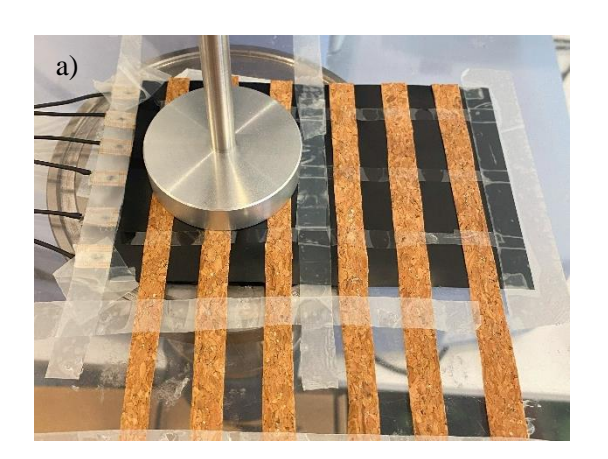


Figure 3.11 - Cork with Velostat grip: a) structure; b) grip mounted on the racket.

3.2.2.1 Pressure Machine Tests with a $R_{bias} = 330 \Omega$

The grip currently under analysis is slightly larger than the paper with Velostat sensor used in Section 3.2.1, as it was subsequently applied to the racket without the need to fabricate a new matrix, thereby avoiding the unnecessary use of additional material. The 6 x 6 matrix used is shown in Figure 3.12, with a resolution of 36 pixels. The pitch length is around 1 cm. It is also possible to note that the force gauge was only able to include half of the sensor array, leading to a split in the sensor for analysis as Figure 3.12 illustrates. The readout circuitry remained unchanged with a R_{bias} of 330 Ω .



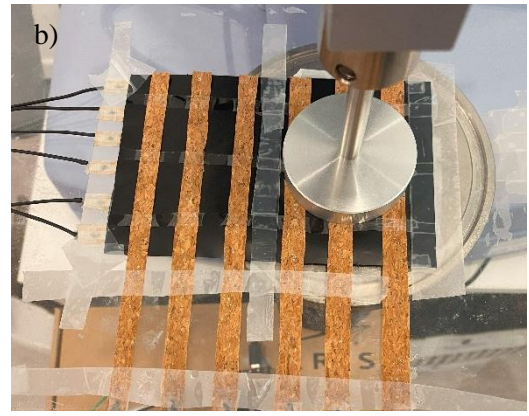
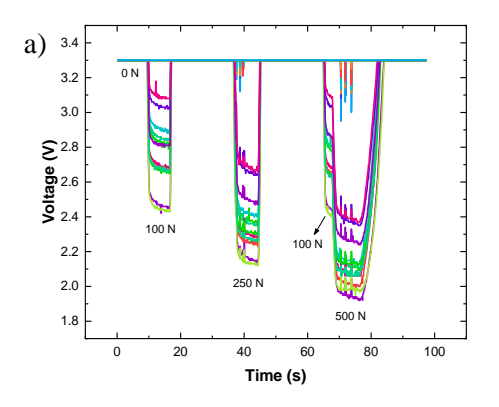


Figure 3.12 - Pressure machine set up for testing of the cork with Velostat grip: a) left side of the sensor; b) right side of the sensor.

3.2.2.1.1 Steps

The plots below, Figure 3.13, represent the grip's response to a sequence of pressures design to simulate a possible chain of actions that could be played during a match. Figure 3.13 a) corresponds to the response of the left side of the sensor, whereas Figure 3.13 b) is linked to the right side of the sensor.



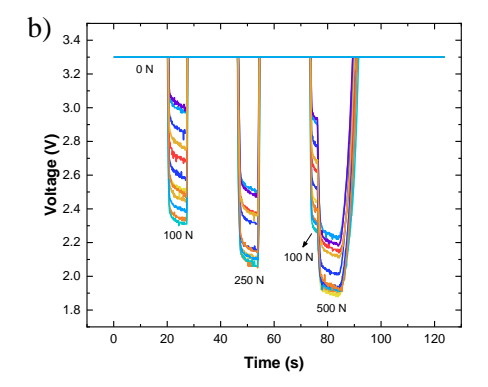


Figure 3.13 – Performance of the smart grip during the Steps test: a) left side of the sensor; b) right side of the sensor.

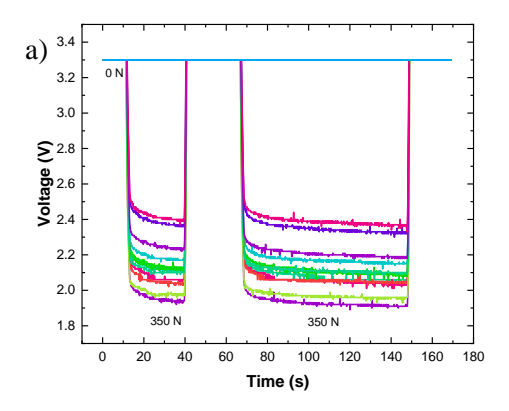
Both sides of the grip had great results with clear define steps in each voltage drop. Regarding the left side of the grip in Figure 3.13 a), a small crosstalk effect can be viewed in the 250 N step and 500 N step. The colouring of the lines reveals that the crosstalk was mainly felt on the right side of the sensor. Again, the cause of "ghost" effect is due to irregularities in the Velostat substrate and current leaks to neighbouring conductive particles, leading to false responses in non-pressed pixels [56]. Despite this occurrence this phenomenon can be overlooked, given the great response of the left side of the sensor. In each step, various lines display a range of voltage drops, which can be attributed to the sensing and pressure distribution. Pixels surrounding the cylinder force gauge suffered decreased voltage drops comparing to the ones directly pressed by the machine as expected. For instance, during the 500 N steps the maximum voltage drop was around 1.4 V while the minimum value was 0.9 V. The left side of the grip displayed similar results to the right as depicted in Figure 3.13 b). The differences in voltage drops are more prominent in the first step, corresponding to a force of 100 N. In this step, the maximum voltage decrease was approximately 1 V, whereas the minimum was 0.3 V. During the remainder of the test, these differences became smaller.

Comparing both plots, it is worth noting the right side response is somewhat more pronounced than the left side. This could be credited to the non-uniformity of the Velostat sheet. A key observation is the curvature and decline in voltage with each step. Since the tests were based on stroke rather than force, the pressure machine constantly adjusted the stroke to the set value, leading to anticipated voltage variations.

3.2.2.1.2 Continuous Pressure

For the Continuous Pressure test, two plots, presented in Figure 3.14, were traced – the left plot linked to the left side of the grip and the right plot corresponding to the right side. Both sides have a similar result, with an average voltage drop of 1.4 V during the entire sequence. Moreover, the left plot showed a higher range of voltage changes, indicating that pixels sensed the applied forced in distinct ways. The pink trace in Figure 3.14 a) experienced a voltage decrease of 0.9 V. However, the purple trace was more affected by the applied force, demonstrating a voltage drop of 1.4 V. Since the cork strips were not completely attached to the Velostat, with only a little bit of scotch tape in between rows, minor movements could happen during tests. This could lead to pixels sensing differently and therefore, different output voltage. Figure 3.14 b) illustrates the same pattern of discrimination, where the output voltage varies depending on the pixel. Nevertheless, this is less noticeable in Figure 3.14 b) than in Figure 3.14 a). In general, CV grip exhibited excellent durability to the prolonged test, indicating that it could be used for extended periods without losing its sensing capabilities.

Similarly to previous test, curving and decreasing of the voltage at the maximum force stage is observed. Since the tests were defined by stroke, instead of force, the pressure machine was always correcting the stroke to the set value. Therefore, changes in the voltage value were expected.



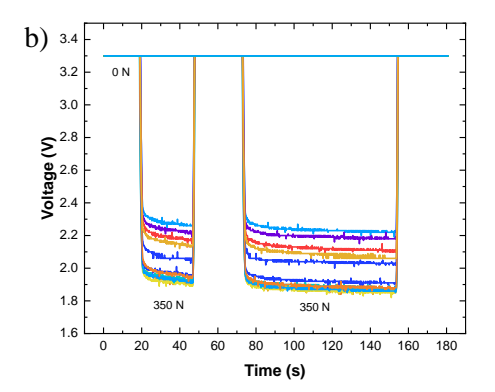
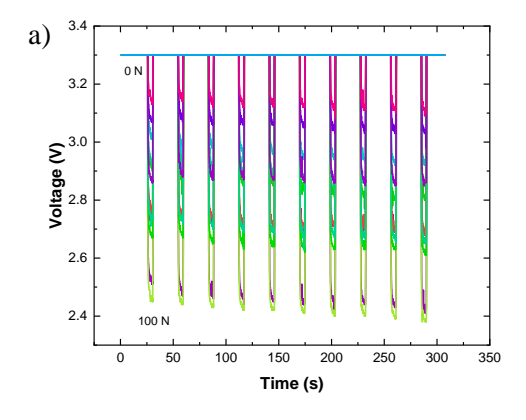


Figure 3.14 - Performance of the smart grip during the Continuous Pressure test: a) left side of the sensor; b) right side of the sensor.

3.2.2.1.3 Cycles 0 to 100 N

The 10 cycles of 0 to 100 N revealed that left side of the sensor detected less pressure than the right side, since it reached a value of 2.4 V (Figure 3.15 a)) while the right side reached a value of 2.3 V (Figure 3.15 b)). This is consistent with the Steps test. This test provides insights into the rapid response of the grip under multiple quick pressings. Some trace lines with higher voltage values in each drop, are observed in both plots as a result of the crosstalk effect and different pressure distribution; however it could be overlooked. The repetitive and periodic nature of the voltage drops and rises indicates a stable and reliable sensor response to the applied force cycles. Comparing the two sides, it is evident that both sides of the sensor behave similarly, with minor variations in the exact voltage values. This consistency indicates that the sensor maintains uniform sensitivity and accuracy across its surface.



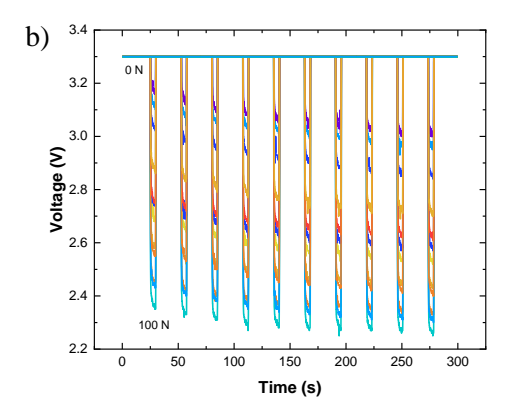
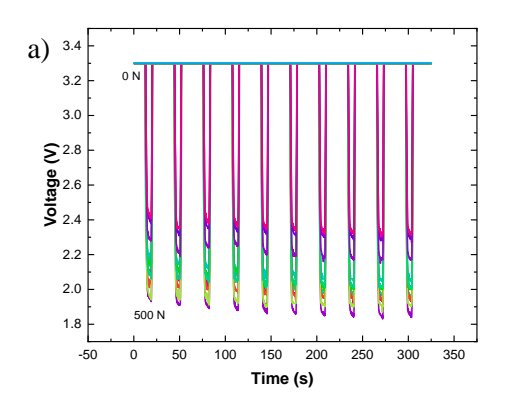


Figure 3.15 - Performance of the smart grip during the Cycle 0 to 100 N test: a) left side of the sensor; b) right side of the sensor.

3.2.2.1.4 Cycles 0 to 500 N

For the present test, similar results were obtained. With a force of 500 N, the decrease in voltage was approximately 1.4 V for the left side of the sensor and 1.5 V for the right side, as shown in Figure 3.16. Here, both sides had practically identical responses, demonstrating that in even with high force values the sensor is reliable and has very low response time, as it responded quickly to the pressure stimulus.



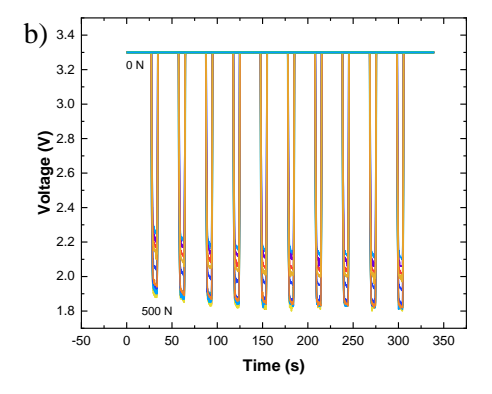


Figure 3.16 - Performance of the smart grip during the Cycle 0 to 500 N test: a) left side of the sensor; b) right side of the sensor.

3.2.2.2 Player-interface evaluation

To gain a deeper understanding of the grip's behaviour in contact with a player's hand, tests were conducted under real-life conditions. The same subjects, previously presented, were gathered to perform assessment tests. Please consult Table 3.2 in Section 3.2.1.2 to see the description and experience level of the participants. In Figure 3.17, the player-interface is displayed, where each player had the chance to hold the racket equipped with the smart grip without using any force first, followed by a maximum force squeeze on the handle. Immediately, it is noticeable that the sensor did not sense the players' hand without any force, shifting from the response in the PV grip. When analysing the second part of Figure 3.17, players 1, 2 and 4 presented a low response, which was expected for participant 1 and 2, as they were inexperienced players, however unlikely for participant 4. Player 3 demonstrated to use the entirety of the matrix, achieving a larger decrease in voltage out of all participants, evident by the darker shades of green. The matrices linked to the other volunteers appeared to be used in sections and not as a whole. This can be attributed to players' hand placement. It is worth noting that the first three players were tested sequentially, whereas player 4 tested the grip within a day of the latter. This allowed the grip to have time to rest and recover completely, making it more difficult to get the same voltage drop as player 3 for instance.



Figure 3.17 - Players performance with the cork with Velostat grip with a R_{bias} of 330 Ω during player-interface evaluation.

All participants showed difficulties in trying to achieve the same voltage drop as they did in prior tests. Owing to the hardness of the cork and its null Poisson ratio, this sensor is more difficult to deform

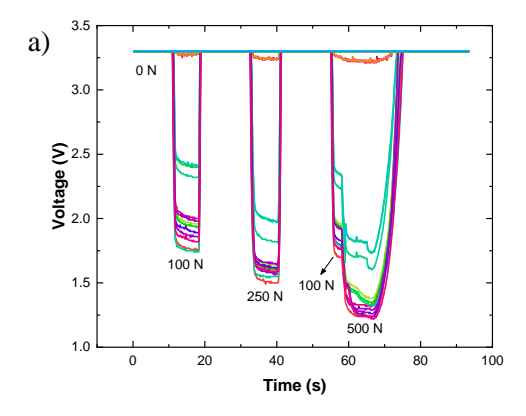
compared to the PV grip when subjected to the same pressure and readout circuitry [44]. Despite the great responsiveness of the grip, the sensitivity was lower than expected, thus it was retested with a R_{bias} of 1 k Ω to improve the sensitivity and consequently, the player-interface evaluation.

3.2.2.3 Pressure Machine Tests with a $R_{bias} = 1 \text{ k}\Omega$

Considering the current state of the art, a 1 $k\Omega$ resistor was selected as the R_{bias} . This allowed the grip to exhibit voltage drops similar to the ones observed in the first sensor (PV grip) under the same pressure. The same tests were reperformed with the new readout circuit.

3.2.2.3.1 Steps

When analysing Figure 3.18, it is possible to see the grip's response to the predefined force sequence. In both sides, the pixels presented a well-defined voltage drop with each force. Slight variations in output signal can be observed, however the grip maintains a stable response throughout the process. In Figure 3.18 a), an orange trace, corresponding to the right side of the sensor, can be detected as result of the crosstalk effect. Nonetheless, since it is such a small drop, it could be discarded. Similar to Section 3.2.2.1.1, both sides of the sensor experienced different sensing in pixels, likely due to uneven pressure distribution. Pixels near the edge of the force gauge were subjected to less pressure than those directly below due to the reduced surface area of the force gauge in contact with those pixels. As a result, pressure distribution varied, causing pixels to display different voltage drops. However, these variations were smaller in this test compared to the Steps test with the CV grip and a $R_{\rm bias} = 330~\Omega$, indicating an improvement in pressure sensing.



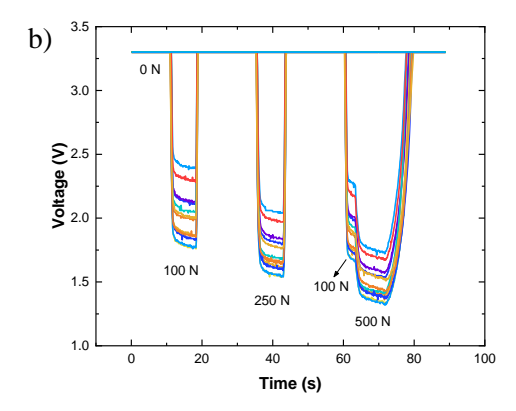


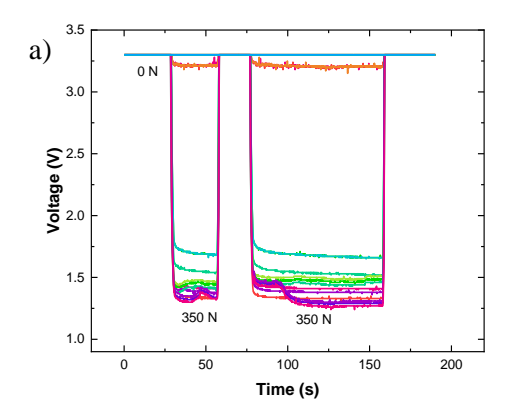
Figure 3.18 - Performance of the smart grip during the Steps test: a) left side of the sensor; b) right side of the sensor.

When the force was applied, Figure 3.18 a) and b) demonstrate a slight curving of the plot and a corresponding decrease in the output signal. This can be attributed to the test settings, where force was applied as a function of stroke. As pressure was applied, the cork deformed, resulting in a stroke value different from the set value. Consequently, the pressure machine continuously corrected the stroke to match the set value, leading to fluctuations in the output signal.

3.2.2.3.2 Continuous Pressure

The results of the Continuous Pressure test are presented in Figure 3.19. Observing Figure 3.19 a), a small variation during the application of force is spotted, especially in the pink and purple traces. This defect never appeared before, suggesting that the likely cause is movement of the table on which the tensile tester was placed. Such movement could potentially interfere with the ongoing test. Additionally, the orange trace, previously seen in the steps test, was observed once again. This line corresponds to pixels in the other half of the sensor which leads to the conclusion that these were results were a by-product of random current flowing through the Velostat sheet.

Both sides demonstrated equal results and improvement from former tests. The range in output voltage has once again decreased significantly, proving that this sensor with the improved readout circuitry is more stable and linear. Moreover, both sides demonstrated a similar voltage drop of around 2.05 V at maximum, responding and recovery very quickly to the applied pressure stimulus. Furthermore, the curving of the plot, seen in previous graphs, appears to be reduced in this test, leading to the conclusion that the sensor signal remains constant under prolonged force.



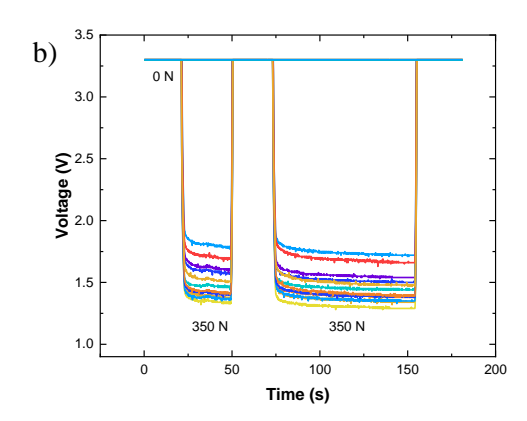
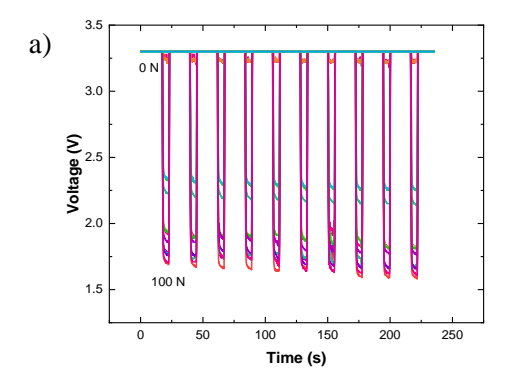


Figure 3.19 - Performance of the smart grip during Continuous Pressure test: a) left side of the sensor; b) right side of the sensor.

3.2.2.3.3 Cycles 0 to 100 N

Figure 3.20 illustrates the results of 10 cycles with a maximum force of 100 N. The left side of sensor array, Figure 3.20 a), exhibited a smaller voltage decrease than the right side, Figure 3.20 b). While Figure 3.20 a) presented a 1.55 V voltage drop, Figure 3.20 b) displayed 1.8 V. This could be attributed to fatigue of the material, since these tests were performed on the same day, or it could be credited to different stroke's value while programming the test. Considering that the force gauge is fixed, the sensor had to be moved to test both sides of the sensor. This means that every change required a redefining of the stroke's value, hence this deviation could be a repercussion of the process. Crosstalk was visible in the left side, indicated by the orange trace near 3.3 V, consistent with observations from previous test. Furthermore, this test demonstrated that the sensor is able to respond quickly to a sequence of force inputs while maintaining precision during testing, a crucial feature for application in padel and tennis.



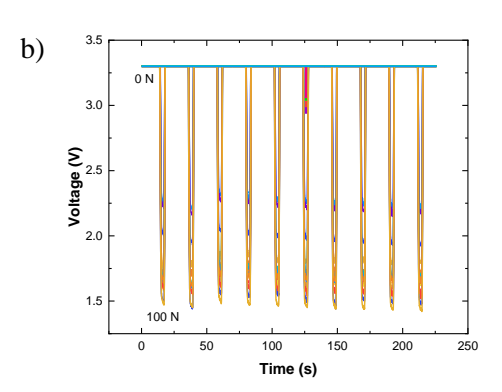
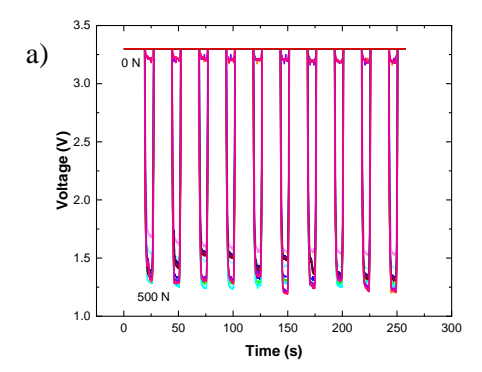


Figure 3.20 - Performance of the smart grip during the Cycle 0 to 100 N test: a) left side of the sensor; b) right side of the sensor.

3.2.2.3.4 Cycles 0 to 500 N

Figure 3.21 shows the results of the 10 cycles, from 0 to 500 N, test. Figure 3.21 a) and b) demonstrate the reliability of this grip, as they show identical results for both sides of the sensor. An average decrease of 2.05 V is noticeable in both plots. The left plot demonstrates variations between cycles, which could be related to the movement of the table where the pressure machine was placed or the uneven placement of the sensor on the machine's base. Nonetheless, the sensor array demonstrated the ability to keep up with the force fluctuations, maintaining a consistent response.



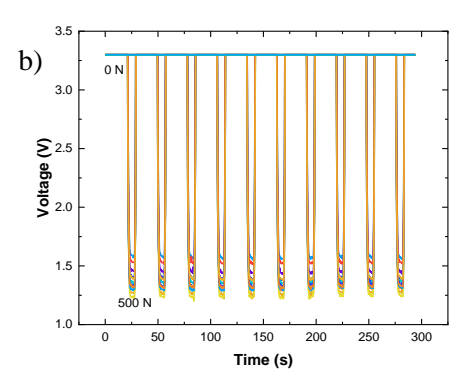


Figure 3.21 - Performance of the smart grip during the Cycle 0 to 500 N test: a) left side of the sensor; b) right side of the sensor.

3.2.2.4 Player-interface evaluation

The same real-life condition tests were implemented. All the variables remained consisted with the previous tests, so please consult Section 3.2.1.2 to gather a detailed description of the subjects and their experience levels. The participants were asked once more to first held the racket with the smart grip without exerting any pressure and then, apply maximum force. Figure 3.22 allows for a comprehensive analysis of the grip's performance under varying levels of force and participants. The main difference from the results presented below and the results with the $R_{\text{bias}} = 330~\Omega$ is the voltage drop achieved by each participant. The matrices under both no force and applied force conditions demonstrate darker shades of green, suggesting that this grip with the $R_{\text{bias}} = 1~k\Omega$ facilitates a greater voltage drop compared to the 330 Ω . When analysing players 1 and 3, it is possible to point that both participants mostly took advantage of the upper part of grip, having a greater voltage drop in the first rows. Adversely, players 2 and 4, both used the grip as whole leading to a uniform response as seen in Figure 3.22.



Figure 3.22 - Players performance with the cork with Velostat grip with a R_{bias} of 1 k Ω during player-interface evaluation.

The grip after testing is illustrated in Annex A.7. This grip did not suffer much tear since the cork is much tougher than paper [47]. Both the strips and Velostat remained nearly intact after the characterization process. This suggests that the smart grip is more durable than the PV grip, and thus, a better option for this application.

3.2.3 Paper with Hydrogel Grip (PH grip)

AlmaScience is a start-up company focused on creating innovative technology based mainly on paper. In search for an even more sustainable option and with the company's goals in mind, a paper grip, that utilizes the great benefits of hydrogels, was designed.

On Figure 3.23, it is possible to observe the PH grip mounted on the racket's handle (Figure 3.23 a)) with its structure schematic on the left (Figure 3.23 b)). New materials were selected for the third grip in hopes to produce a sensor with greener resources. Considering that the hydrogel droplets are more resistive than the Velostat sheet, a resistor 470 k Ω was first used as the R_{bias} for this grip. This value of resistance was based on those studies mentioned above. In the subsequent section, the performance and the durability of the wearable is tested and assessed.

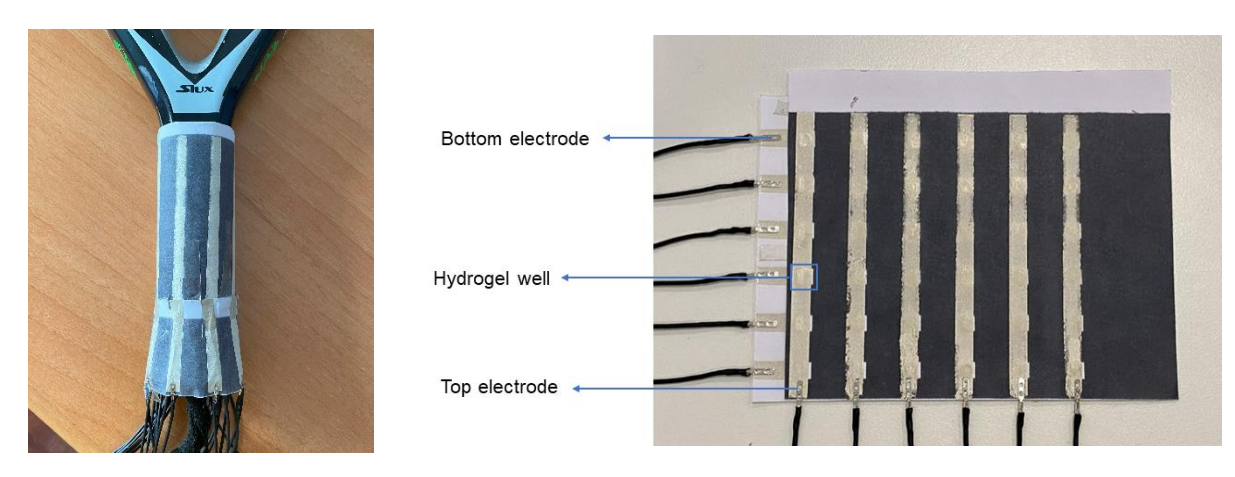


Figure 3.23 - Paper with hydrogel grip: a) grip mounted on the racket; b) structure.

3.2.3.1 Pressure Machine Tests

A 6 x 6 preliminary matrix of the grip was used in the pressure machine tests, as shown in Figure 3.24. 36 pixels, with a pixel pitch of 1 cm, were carefully analysed during the following test: Steps; Continuous Pressure; Cycles 0 to 100 N and Cycles 0 to 500 N. Although the force gauge did not encompass the whole sensor, the decision to split the sensor into two was not made, as it would have caused repetitive responses for pixels that were pressed in both sides.

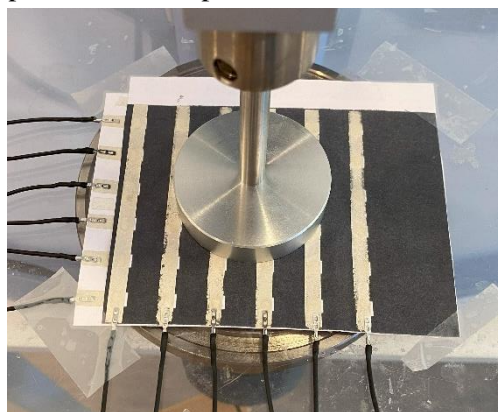


Figure 3.24 - Pressure machine set up for testing of the paper with hydrogel grip.

3.2.3.1.1 Steps

Figure 3.25 represents the output voltage values of the PH grip in function of time and force. As mentioned before, it is worth to emphasize that the forces applied were carefully chosen to represent a possible sequence in a match of padel, such as a volley, followed by a forehand and finished by a smash.

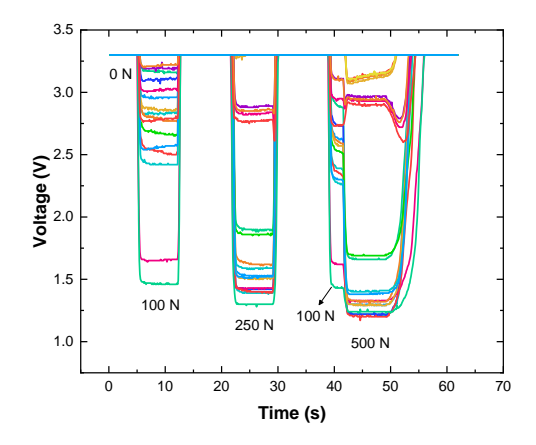


Figure 3.25 - Performance of the smart grip during the Steps test.

For the PH grip, the crosstalk effect was significantly prominent as observed in Figure 3.25. Despite the ability to discriminate between each step, the extent of the "ghost" effect may pose a problem, since non-pressed pixels responded to the force. This could be explained by the pitch length, *i.e.*, the distance between each pixel is too small to create a clean output signal, causing the pixels to sense even if not pressed. In the 500 N step, a slower recovery time is detected, made evident mostly by the green and pink traces which take longer to achieve the baseline. Additionally, in the last step, some pixels experienced a voltage drop of approximately 0.3 V, while others exhibited 2.05 V. Consistent voltage variations can be observed in all steps, suggesting that the sensor experienced uneven pressure distribution. This pattern was also observed in previous tests and grips, likely due to the force gauge's diameter being too small to fully cover the sensor, resulting in uneven pressure application.

3.2.3.1.2 Continuous Pressure

A similar sensing response is seen in the Continuous Pressure test. By analysing the plot of Figure 3.26, the fluctuations in voltage drops can be observed, although less severe than in the previous test. In both presses, the recovery time of the sensor is higher than the response time, leading to the conclusion that the sensor saturates with prolonged applied force. Since the players do not apply force for 180 s or even 60 s, this discrepancy is not so important. Despite its slower recovery time, the output signal remained stable throughout the test, indicating that the sensor is capable of withstanding prolonged pressures.

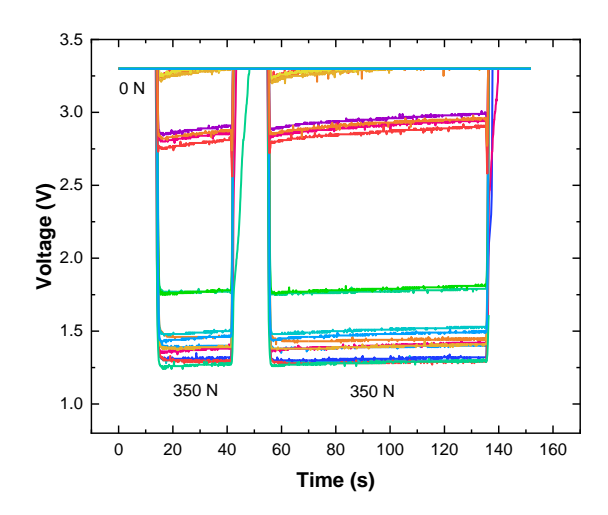


Figure 3.26 - Performance of the smart grip during the Continuous Pressure test.

3.2.3.1.3 Cycles 0 to 100 N

The grip underwent 10 cycles of rapid force application, ranging from 0 to 100 N. Figure 3.27 presents the results of this test. Although there are significant voltage variations, the lowest voltage drop in each cycle was around 1.8 V, consistent throughout the test. The high level of variations in the output voltage suggest that the hydrogels are affected by the surface area in contact with the sensor. In the Continuous Pressure test, it was observed that the response time was smaller than the recovery time. However, in this test, this is not verified. This suggests that the sensor becomes unstable and exhibits slower response under constant force but remains reliable during the rapid application of forces. The game of padel and tennis do not have moments where athletes apply continuous pressure for long periods of time, therefore this aspect is not an immediate issue. Nonetheless, this leaves questions in terms of longevity. Figure 3.27 demonstrates that the sensor is able to respond to quick pressures, which is vital for this application.

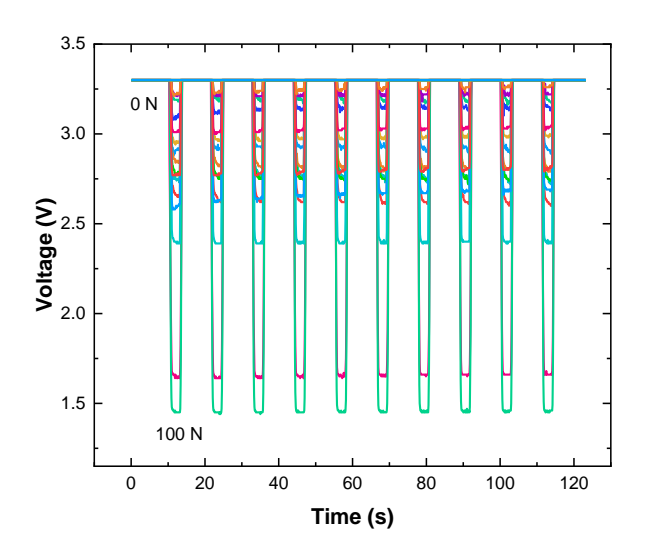


Figure 3.27 - Performance of the smart grip during the Cycles 0 to 100 N test.

3.2.3.1.4 Cycles 0 to 500 N

The grip responded identically to this test as observed in Figure 3.28. Here the variations in output signal are not so noticeable as they are, in lower pressures. Additionally, a consistent drop in voltage is achieved in each cycle, averaging a 2.05 V. Despite the slight variation in the output signal, this sensor's response indicates that the wearable is considerably stable and linear.

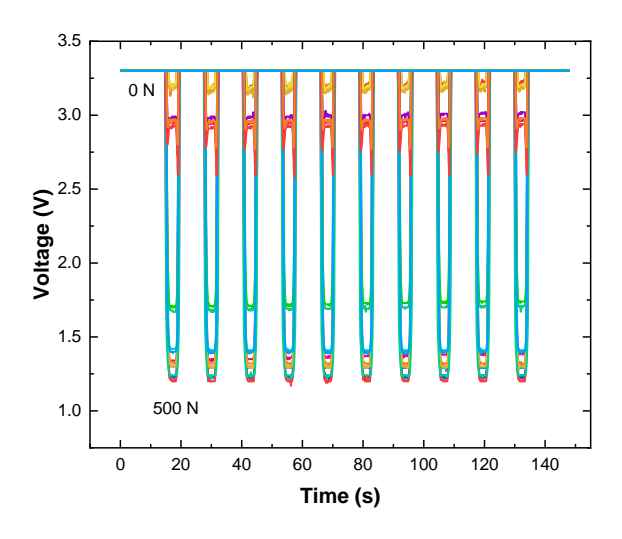


Figure 3.28 - Performance of the smart grip during the Cycles 0 to 500 N test.

In conclusion, the PH grip presents some limitations that could be improved with a bigger pitch length or, for instance, slight adjustments to the hydrogel composition. These modifications could reduce its sensitivity to pressure, potentially resulting in fewer variations in the output signal.

3.2.3.2 Player-interface evaluation

Upon testing the grip in the first player, it was quickly realized that grip was already responding even without applied force, generating a matrix image where all pixels had a value of 0 V. The sensor was tested with a player right after the pressure machine tests, so it did not have time to rest and, hence,

recover completely. This was believed to be the reason behind these results. Therefore, the grip was then let to rest for a few hours before continuing the test.

Later, the same results were observed, however nothing had been changed or broken, meaning that due to the dynamic measurements the grip suffered wear and tear. This also indicated that the grip became slightly less resistive, so a new R_{bias} of 10 k Ω was employed. The player-interface evaluations were carried out with this new load resistor. Figure 3.29 provides the generated pictures of each player.



Figure 3.29 - Players performance with the paper with hydrogel grip during player-interface evaluation.

The second, third and fourth players displayed similar results, having a little response in the first part of the test (without force) and reaching low voltage values in the second part (with force). Player 2 and 3 used essentially the upper part of the grip while player 4 applied force, mainly, to the middle of the sensor. Player 1 results were inconsistent with the rest. Even without applying force, the sensor was already responding. Moreover, it can be observed that column 5 did not show any voltage drop when pressure was applied. There is a possibility that the player's hand was sweatier than the others. The sweat causes the hydrogel to swell, increasing its conductivity and resulting in higher sensitivity. Despite the grip's limitations, the handprints of players 2, 3, and 4 are clearly visible in the generated matrices, indicating that valuable feedback on hand positioning can still be provided to the players.

The grip after testing is shown in Annex A.8. This grip prototype suffered wear and tear due to the fragile nature of the paper. Despite the absence of tears from use, it was visible that the grip was deformed with each test. This deformation was especially predominant during the player-interface evaluation, where each player had a specific way to grip the racket, therefore, denting the grip even more. In addition, the hydrogel droplets exhibited challenges in performance due to sweat from the players' hand. As the application is intended for players during training, this grip may not be the most suitable option for this purpose. Similarly to the PV grip, one potential improvement could involve covering the smart grip with an overgrip to offer added protection. However, this solution was not explored in the current testing, indicating that further evaluation is needed.

3.2.4 Grip comparison

In this section, an estimate of the sensitivity values of the grips are determined, followed by a comprehensive overview of the characterization of the grips.

Using the output signals values of 5 pixels from the Steps tests of each grip, the sensitivity of each pixel was determined with Equation (2)

$$S = \frac{d(\frac{\triangle R}{R_0})}{dP} \tag{2}$$

where $\triangle R$ corresponds to the resistance change, R_0 is the initial resistance of each sensor when an initial pressure of 51 kPa is applied and P is the compressive pressure. Subsequently, the average of these sensitivities was calculated to estimate the overall average sensitivity of the entire sensor.

Figure 3.30 displays the relative resistance change of each grip. In the graph it is possible to note four distinct sections of the sensor behaviour under increasing pressure. In the first section, the plot remains at 0, as the sensors are electrically resistive when no pressure is applied. The second section, between 51 kPa and 127 kPa, shows a decrease in sensitivity due to the compression of the active materials. In the case of Velostat, the compression brings the carbon particles closer together, allowing conduction to begin. For the hydrogel droplets, the compression causes a similar conduction effect, ultimately reducing resistance. In the third section, where pressure is even higher, further compression of the active materials occur. However, as the particles in both the Velostat and hydrogel droplets are already in contact, the relative resistance change is much smaller. Finally, in the fourth section, the Velostat and the hydrogel droplets reach saturation, meaning the relative resistance change remains stable, as further pressure does not affect conduction. Therefore, two distinct pressure ranges characterized by different sensitivities can be recognized: a low-pressure range from 51 kPa to 127 kPa (S₁) and high-pressure range from 127 kPa to 255 kPa (S₂).

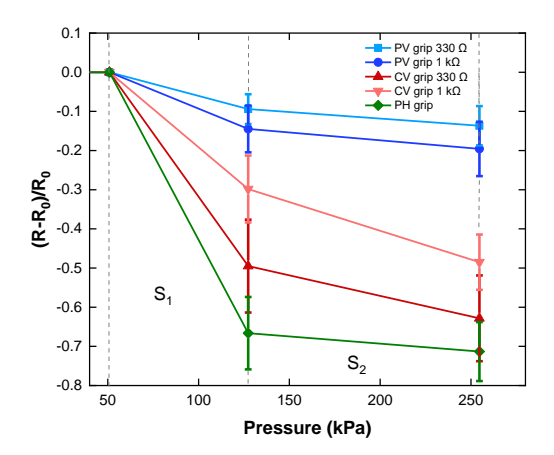


Figure 3.30 - Relative resistance change for each grip, under pressures ranging from 51 kPa to 255 kPa.

Table 3.3 indicates the average sensitivity values for each grip. As previously discussed, the sensitivities in the S_2 range are expected to be lower than in the S_1 range, as the active materials are already compressed and approaching saturation. Among the grips, the CV grip with a R_{bias} of 330 Ω and PH grip exhibit the highest values of sensitivity in both S_1 and S_2 . The elevated sensitivity in the PH grip was expected, since hydrogel is commonly employed to enhance sensitivity in flexible pressure sensors. The calculations of the pressures and sensitivity values are displayed in Annex A.9. It is important to emphasize that the presented sensitivity values represent an estimate of the sensors' performance, and further in-depth studies are necessary to validate these findings.

Table 3.3 - Average sensitivity values for the pressure ranges S₁ and S₂ of each grip.

	SENSIVITY (MPa ⁻¹)			
	S_1 S_2			
PV grip with 330 Ω	-1 ± 0.5	-1 ± 0.2		
PV grip with $1 \text{ k}\Omega$	-2 ± 0.8	-1 ± 0.3		
CV grip with 330 Ω	-6 ± 2	-3 ± 1		
CV grip with $1 \text{ k}\Omega$	-4 ± 1	-2 ± 0.4		
PH grip	-9 ± 1	-4 ± 0.4		

In Table 3.4, a summarized overview of the smart grips fabricated in this work is presented. It provides a comparative analysis of the three grip designs, focusing on their structure, performance, durability, and estimated price. This overview offers insight into the key attributes of each grip type, highlighting their respective strengths and limitations across different evaluation criteria.

Table 3.4 - Overview of the smart grips studied in this work.

	STRUCTURE	PERFORMANCE	DURABILITY	ESTIMATED PRICE*1
Paper with Velostat grip	Velostat - active material Paper – substrate Silver tracks – electrodes	 Consistent output signal in Continuous pressure test, cycles tests and player evaluations. Saturates at 250 N, unable to differentiate higher forces. 	Suffered significant wear and tear, especially in the electrodes	≈ 1.11 €
Cork with Velostat grip	Velostat – active material Cork – substrate Silver tracks – electrodes	 Excellent results, consistent output signal in all tests. Can distinguish different forces and responded rapidly in the cycles tests Showed dynamic range in player-interface evaluations. 	Very durable, no signs of wear and tear	≈ 2.05 €
Paper with hydrogel grip	Hydrogel – active material Paper - substrate Silver tracks - electrodes	 Can distinguish forces but slower recovery in some tests. Affected by sweat during player evaluations. 	Suffered wear and tear	≈ 1.01 €

^{*1-} estimate price of a single unit. The calculations for these prices are demonstrated in Annex A.10

CONCLUSIONS AND FUTURE PERSPECTIVES

In this study, different materials were used to create a smart grip for tennis and padel rackets. A smart grip can be viewed as a wearable tactile sensor, since its aim is to measure grip strength and recognize hand position. This grip is intended to be implemented in the racket's handle, therefore the materials chosen must fulfilled all the required criteria such as pressure sensitivity, flexibility to ensure it is conformable to the handle and mechanical and structural strength to guarantee that the smart grip can withstand the aggressive handling. The pressure sensing methods used for this application were piezoresistive due to their great advantages in wearable technology.

Velostat was chosen as the piezoresistive material due to its remarkable properties. It is embedded with carbon black particles, which confer interesting piezoresistive characteristics such as quantum tunnelling and percolation properties, making it one of the most reliable materials for tactile sensors. Moreover, Velostat is a cost-effective material, and it is also flexible, as it is a thin, plastic-like sheet that can easily conform to different surfaces. In addition to this, it possesses significant mechanical and structural strength, enabling it to endure a broad range of pressures. Velostat is also sensitive to both light and heavy touch, making it an ideal choice for this application as different strokes in padel/tennis require different forces.

For the third grip, hydrogels were synthesized from Na-CMC, CaCl₂ and ZnCl₂. This sustainable material presents significant advantages, including, elasticity and an increased contact area, making it an innovative material in the field of piezoresistive sensors. These hydrogels stand out from the state of the art for being the dielectric layer. Their novel application in this context, highlight their potential, particularly given their mechanical properties. However, despite being dried, they exhibited high susceptibility to humidity, posing a challenge for the smart grip, where they will be exposed to sweat during gameplay or practice. This vulnerability can be overcome with the incorporation of an additional protective layer to ensure the hydrogels maintain their integrity and functionality in these conditions.

The smart grip was designed with a three-layer structure. The top and bottom layers functioned as electrodes, oriented at 90° to each other to create a matrix configuration, with a sensing layer positioned between. To align with the sustainability goals of this thesis, both paper and cork, featuring screen-printed Ag tracks, were studied as materials for the electrode layers. Moreover, these substrates are low cost and very easy to manipulate and adapt to any surface which enables fast production of wearables.

Three different grips were fabricated and characterized. The first grip, made with patterned paper and Velostat, exhibited great results in the mechanical tests, with a R_{bias} = 330 Ω . It maintained consistent output signal under prolonged forces in the Continuous Pressure test and under fast forces in cyclic tests. However, it was noticeable that this grip could not discriminate forces above 250 N, as the voltage drop remained similar across tests involving different force levels. Moreover, the sensor's performance was slightly affected by the "ghost" effect, as some pixels were sensing when no pressure was applied. Additionally, the screen-printed paper strips tore during the real-life testing, leading to partial disconnection of the smart grip. As a result, it was concluded that this grip is not fully suitable for this

application. During gameplay, players can exert greater forces in certain strokes, which would not be possible to accurately identify in the feedback, given these results.

In the second grip, the patterned paper was replaced with screen-printed cork to ensure the durability of the electrodes as cork is more resilient than paper. This smart grip was initially tested with a $R_{\text{bias}} = 330~\Omega$. Despite the favourable results in the pressure machine tests, the players had difficulty in decreasing the voltage while applying force, during the real-life test. As a result, the tests were repeated with a $R_{\text{bias}} = 1~k\Omega$ to improve sensitivity. The smart grip exhibited excellent performance with the new R_{bias} in both the mechanical tests and the real-life testing. Players did not experience the same difficulties as before, finding it much easier to reduce the voltage with the new circuitry. The cork with Velostat grip presented the best results among the three grips created.

The third grip, consisting of hydrogels droplets sandwiched between two screen-printed papers with Ag lines, require a significantly higher R_{bias} due to the hydrogels' high internal resistance, leading to the use of a 470 k Ω resistor. Mechanical tests results indicated that this grip was affected by the crosstalk effect, with output voltage drops occurring in pixels that were not pressed. Although the sensor recovered quickly in the dynamic measurements, it later exhibited signs of fatigue, producing unusual results during real-life testing. Furthermore, the smart grip's performance was highly influenced by the humidity in the players' hands during the real-life tests, resulting in an overly sensitive sensor.

The grips produced in this study offer significant improvements over those discussed in existing literature. There is a noticeable gap in research specifically focused on enhancing padel and tennis gameplay by extracting data from the players' hands which highlighting the novelty of this work. Moreover, the grips developed in this study follow a continuous sensing surface design, which is a critical advancement for this type of wearable, as most of the existing sensors are design in a single-pixel structure typically placed at strategic points. This leads to a more universal grip, since each player grips the handle differently. Finally, the real-time data feedback provided by these grips addresses the needs and desires of athletes, offering immediate and actionable insights during gameplay.

Future research should focus on miniaturizing the readout circuitry to implement it either at the butt of the racket or in the heart of the racket. Another approach to this could be implementing the circuitry inside the handle. However, that would require it to occur during the production of the racket which would increase the cost and difficulty of the application. This innovation would also benefit from testing in extreme conditions to gain a deeper understanding of the grip's durability and longevity. Moreover, an extensive study of the sensors' sensitivity would provide valuable insights. Additionally, different compositions of the hydrogels could be attempted to optimize the recovery results. To reduce costs, future work could explore replacing the screen-printed Ag ink with screen-printed C ink. Furthermore, increasing the resolution of the grip could enable the capture of a cleaner handprint, enhancing the detail and accuracy of the sensor. In addition, implementing wireless connectivity would allow for real-time data transmission, further improving the effectiveness of the smart grip during gameplay. Additionally, integrating IoT technology to connect the racket to a processing unit, possessing accelerometers and gyroscopes, in a consistent manner to not only acquire real-time data related to hand position and grip strength, but also to gather data regarding ball velocity, player location, etc. Studying and completing these future perspectives could revolutionize the wearables in padel and tennis to enhance gameplay.

BIBLIOGRAPHY

- [1] L. Buthe, U. Blanke, H. Capkevics, and G. Troster, "A wearable sensing system for timing analysis in tennis," in 2016 IEEE 13th International Conference on Wearable and Implantable Body Sensor Networks (BSN), IEEE, Jun. 2016, pp. 43–48. doi: 10.1109/BSN.2016.7516230.
- [2] J. Williamson *et al.*, "Data sensing and analysis: Challenges for wearables," in *The 20th Asia and South Pacific Design Automation Conference*, IEEE, Jan. 2015, pp. 136–141. doi: 10.1109/ASPDAC.2015.7058994.
- [3] N. Niknejad, W. B. Ismail, A. Mardani, H. Liao, and I. Ghani, "A comprehensive overview of smart wearables: The state of the art literature, recent advances, and future challenges," *Eng. Appl. Artif. Intell.*, vol. 90, no. January, p. 103529, 2020, doi: 10.1016/j.engappai.2020.103529.
- [4] M. Rana and V. Mittal, "Wearable Sensors for Real-Time Kinematics Analysis in Sports: A Review," *IEEE Sens. J.*, vol. 21, no. 2, pp. 1187–1207, 2021, doi: 10.1109/JSEN.2020.3019016.
- [5] M. J. McGrath and C. N. Scanaill, "Sensor Network Topologies and Design Considerations," in *Sensor Technologies*, 2013, pp. 79–95. doi: 10.1007/978-1-4302-6014-1_4.
- [6] G. Aroganam, N. Manivannan, and D. Harrison, "Review on Wearable Technology Sensors Used in Consumer Sport Applications," *Sensors*, vol. 19, pp. 1–26, 2019.
- [7] L. Coorevits and T. Coenen, "The rise and fall of wearable fitness trackers," *Acad. Manag. Proc.*, vol. 2016, no. 1, p. 17305, 2016, doi: 10.5465/ambpp.2016.17305abstract.
- [8] S. McDevitt *et al.*, "Wearables for Biomechanical Performance Optimization and Risk Assessment in Industrial and Sports Applications," *Bioengineering*, vol. 9, no. 1, 2022, doi: 10.3390/bioengineering9010033.
- [9] L. T. Vidal, H. Zhu, A. Waern, and E. M. Segura, "The design space of wearables for sports and fitness practices," *Conf. Hum. Factors Comput. Syst. Proc.*, 2021, doi: 10.1145/3411764.3445700.
- [10] D. Connaghan *et al.*, "A Sensing Platform for Physiological and Contextual Feedback to Tennis Athletes," *2009 Sixth Int. Work. Wearable Implant. Body Sens. Networks*, pp. 224–229, 2009, doi: 10.1109/bsn.2009.63.
- [11] N. Cavdar Aksoy, A. Kocak Alan, E. Tumer Kabadayi, and A. Aksoy, "Individuals' intention to use sports wearables: the moderating role of technophobia," *Int. J. Sport. Mark. Spons.*, vol. 21, no. 2, pp. 225–245, 2020, doi: 10.1108/IJSMS-08-2019-0083.
- [12] M. H. Iqbal, A. Aydin, O. Brunckhorst, P. Dasgupta, and K. Ahmed, "A review of wearable technology in medicine," *J. R. Soc. Med.*, vol. 109, no. 10, pp. 372–380, 2016, doi: 10.1177/0141076816663560.
- [13] W. L. Wu *et al.*, "Creating a scoring system with an armband wearable device for table tennis forehand loop training: Combined use of the principal component analysis and artificial neural network," *Sensors*, vol. 21, no. 11, pp. 1–13, 2021, doi: 10.3390/s21113870.
- [14] T. Yamashita and T. Kobayashi, "Smart ping pong racket by ultrathin piezoelectric strain sensor array," *Symp. Des. Test, Integr. Packag. MEMS/MOEMS*, *DTIP 2018*, pp. 1–3, 2018, doi: 10.1109/DTIP.2018.8394237.
- [15] P. Blank, T. Kautz, and B. M. Eskofier, "Ball impact localization on table tennis rackets using piezo-electric sensors," *Int. Symp. Wearable Comput. Dig. Pap.*, pp. 72–79, 2016, doi: 10.1145/2971763.2971778.

- [16] V. Ferraro, "Smart Textiles and Wearable Technologies for Sportswear: A Design approach.," *Sensors*, 2015, doi: 10.3390/ecsa-2-s3005.
- [17] M. R. Ebling, "IoT: From Sports to Fashion and Everything In-Between," *IEEE Pervasive Comput.*, vol. 15, no. 4, pp. 2–4, 2016, doi: 10.1109/MPRV.2016.71.
- [18] H. Zhao, S. Wang, G. Zhou, and W. Jung, "Tenniseye: Tennis ball speed estimation using a racket-mounted motion sensor," *IPSN 2019 Proc. 2019 Inf. Process. Sens. Networks*, pp. 241–252, 2019, doi: 10.1145/3302506.3310404.
- [19] C. J. Ebner and R. D. Findling, "Tennis Stroke Classification: Comparing Wrist and Racket as IMU Sensor Position," *ACM Int. Conf. Proceeding Ser.*, pp. 74–83, 2019, doi: 10.1145/3365921.3365929.
- [20] E. M. Keaney and M. Reid, "Quantifying hitting activity in tennis with racket sensors: new dawn or false dawn?," *Sport. Biomech.*, vol. 19, no. 6, pp. 831–839, 2020, doi: 10.1080/14763141.2018.1535619.
- [21] C. Espino Palma, V. Luis del Campo, and D. Muñoz Marín, "Visual Behaviours of Expert Padel Athletes When Playing on Court: An In Situ Approach with a Portable Eye Tracker," *Sensors*, vol. 23, no. 3, 2023, doi: 10.3390/s23031438.
- [22] A. García-Giménez, F. Pradas de la Fuente, C. Castellar Otín, and L. Carrasco Páez, "Performance Outcome Measures in Padel: A Scoping Review," *Int. J. Environ. Res. Public Health*, vol. 19, no. 7, 2022, doi: 10.3390/ijerph19074395.
- [23] F. Pradas, A. Sánchez-Pay, D. Muñoz, and B. J. Sánchez-Alcaraz, "Gender differences in physical fitness characteristics in professional padel players," *Int. J. Environ. Res. Public Health*, vol. 18, no. 11, 2021, doi: 10.3390/ijerph18115967.
- [24] F. Pradas, V. Toro-Román, M. Á. Ortega-Zayas, D. M. Montoya-Suárez, B. J. Sánchez-Alcaraz, and D. Muñoz, "Physical Fitness and Upper Limb Asymmetry in Young Padel Players: Differences between Genders and Categories," *Int. J. Environ. Res. Public Health*, vol. 19, no. 11, 2022, doi: 10.3390/ijerph19116461.
- [25] E. Li, X. Lin, B. C. Seet, F. Joseph, and J. Neville, "Low profile and low cost textile smart mat for step pressure sensing and position mapping," *I2MTC 2019 2019 IEEE Int. Instrum. Meas. Technol. Conf. Proc.*, vol. 2019-May, pp. 1–5, 2019, doi: 10.1109/I2MTC.2019.8826892.
- [26] M. Gala, J. Barabas, and M. Kopaskova, "User presence monitoring based on Velostat pressure sensors and Arduino platform," *Proc. 2020 IEEE 21st Int. Conf. Comput. Probl. Electr. Eng. CPEE 2020*, pp. 6–8, 2020, doi: 10.1109/CPEE50798.2020.9238739.
- [27] S. Krizkova, H. Tomaskova, and E. B. Tirkolaee, "Sport performance analysis with a focus on racket sports: A review," *Appl. Sci.*, vol. 11, no. 19, 2021, doi: 10.3390/app11199212.
- [28] S. Emamian, B. B. Narakathu, A. A. Chlaihawi, B. J. Bazuin, and M. Z. Atashbar, "Screen printing of flexible piezoelectric based device on polyethylene terephthalate (PET) and paper for touch and force sensing applications," *Sensors Actuators, A Phys.*, vol. 263, pp. 639–647, 2017, doi: 10.1016/j.sna.2017.07.045.
- [29] E. Pritchard, M. Mahfouz, B. Evans, S. Eliza, and M. Haider, "Flexible capacitive sensors for high resolution pressure measurement," *Proc. IEEE Sensors*, pp. 1484–1487, 2008, doi: 10.1109/ICSENS.2008.4716726.
- [30] I. Vehec and L. Livovsky, "Flexible Resistive Sensor Based on Velostat," *43rd Int. Spring Semin. Electron. Technol.*, vol. 2020-May, pp. 1–6, 2020, doi: 10.1109/ISSE49702.2020.9121009.
- [31] A. Dzedzickis *et al.*, "Polyethylene-carbon composite (Velostat®) based tactile sensor," *Polymers (Basel).*, vol. 12, no. 12, pp. 1–17, 2020, doi: 10.3390/polym12122905.
- [32] M. Hopkins, R. Vaidyanathan, and A. H. McGregor, "Examination of the Performance Characteristics of Velostat as an In-Socket Pressure Sensor," *IEEE Sens. J.*, vol. 20, no. 13, pp. 6992–7000, 2020, doi: 10.1109/JSEN.2020.2978431.
- [33] J. Qin *et al.*, "Flexible and Stretchable Capacitive Sensors with Different Microstructures," *Adv. Mater.*, vol. 33, no. 34, pp. 1–31, 2021, doi: 10.1002/adma.202008267.
- [34] S. S. Suprapto, A. W. Setiawan, H. Zakaria, W. Adiprawita, and B. Supartono, "Low-Cost Pressure Sensor Matrix Using Velostat," *Proc.* 2017 5th Int. Conf. Instrumentation, Commun. Inf. Technol. Biomed. Eng. ICICI-BME 2017, no. November, pp. 137–140, 2018, doi:

- 10.1109/ICICI-BME.2017.8537720.
- [35] T. Li *et al.*, "A flexible pressure sensor based on an MXene-textile network structure," *J. Mater. Chem. C*, vol. 7, no. 4, pp. 1022–1027, 2019, doi: 10.1039/c8tc04893b.
- [36] M. Li *et al.*, "Flexible conductive hydrogel fabricated with polyvinyl alcohol, carboxymethyl chitosan, cellulose nanofibrils, and lignin-based carbon applied as strain and pressure sensor," *Int. J. Biol. Macromol.*, vol. 166, pp. 1526–1534, 2021, doi: 10.1016/j.ijbiomac.2020.11.032.
- [37] S. K. Mahadeva, K. Walus, and B. Stoeber, "Piezoelectric paper for physical sensing applications," in 2015 28th IEEE International Conference on Micro Electro Mechanical Systems (MEMS), IEEE, Jan. 2015, pp. 861–864. doi: 10.1109/MEMSYS.2015.7051095.
- [38] B. J. Park, S. Oh, F. S. Kim, and S. T. Chang, "Pixel-free capacitive touch sensor using a single-layer ion gel," *J. Mater. Chem. C*, vol. 7, no. 33, pp. 10264–10272, 2019, doi: 10.1039/c9tc02809a.
- [39] N. Cameron, "ESP32 Microcontroller," in *ESP32 Formats and Communication: Application of Communication Protocols with ESP32 Microcontroller*, Berkeley, CA: Apress, 2023, pp. 1–54. doi: 10.1007/978-1-4842-9376-8 1.
- [40] D. dos Santos de Abreu, M. Strauss, and M. Santhiago, *Flexible cellulose-based devices for monitoring physical parameters*, 1st ed., vol. 89. Elsevier B.V., 2020. doi: 10.1016/bs.coac.2020.01.002.
- [41] H. Zhou *et al.*, "Capacitive Pressure Sensors Containing Reliefs on Solution-Processable Hydrogel Electrodes," *ACS Appl. Mater. Interfaces*, vol. 13, no. 1, pp. 1441–1451, 2021, doi: 10.1021/acsami.0c18355.
- [42] A. Eshkeiti *et al.*, "Screen printed flexible capacitive pressure sensor," *IEEE Sensors*, pp. 1192–1195, 2014, doi: 10.1109/ICSENS.2014.6985222.
- [43] H. Yu, H. Han, J. Jang, and S. Cho, "Fabrication and Optimization of Conductive Paper Based on Screen-Printed Polyaniline/Graphene Patterns for Nerve Agent Detection," *ACS Omega*, vol. 4, no. 3, pp. 5586–5594, 2019, doi: 10.1021/acsomega.9b00371.
- [44] H. Harija *et al.*, "A Piezoresistive Cork-Based Sustainable and Robust Sensor for Force-Sensing Application," *IEEE Sens. J.*, 2024, doi: 10.1109/JSEN.2024.3448632.
- [45] S. L. Silvestre *et al.*, "Cork derived laser-induced graphene for sustainable green electronics," *Flex. Print. Electron.*, vol. 7, no. 3, 2022, doi: 10.1088/2058-8585/ac8e7b.
- [46] A. F. Carvalho, A. J. S. Fernandes, R. Martins, E. Fortunato, and F. M. Costa, "Laser-Induced Graphene Piezoresistive Sensors Synthesized Directly on Cork Insoles for Gait Analysis," *Adv. Mater. Technol.*, vol. 5, no. 12, pp. 1–8, 2020, doi: 10.1002/admt.202000630.
- [47] H. Harija *et al.*, "Novel Cork-based Laser-Induced Graphene Sensors: Proof-of-Concept and Initial Results," *Proc. Int. Conf. Sens. Technol. ICST*, pp. 1–6, 2023, doi: 10.1109/ICST59744.2023.10460839.
- [48] M. Gerometta, X. Gabrion, A. Lagorce, S. Thibaud, and T. Karbowiak, "Towards better understanding of the strain–stress curve of cork: A structure–mechanical properties approach," *Mater. Des.*, vol. 235, no. June, 2023, doi: 10.1016/j.matdes.2023.112376.
- [49] H. Zhou *et al.*, "Robust and sensitive pressure/strain sensors from solution processable composite hydrogels enhanced by hollow-structured conducting polymers," *Chem. Eng. J.*, vol. 403, p. 126307, 2021, doi: 10.1016/j.cej.2020.126307.
- [50] G. Ge *et al.*, "Stretchable, Transparent, and Self-Patterned Hydrogel-Based Pressure Sensor for Human Motions Detection," *Adv. Funct. Mater.*, vol. 28, no. 32, pp. 1–8, 2018, doi: 10.1002/adfm.201802576.
- [51] C. C. Kim, H. H. Lee, K. H. Oh, and J. Y. Sun, "Highly stretchable, transparent ionic touch panel," *Science* (80-.)., vol. 353, no. 6300, pp. 682–687, 2016, doi: 10.1126/science.aaf8810.
- [52] P. T. Hoang, H. Phung, C. T. Nguyen, T. Dat Nguyen, and H. R. Choi, "A highly flexible, stretchable and ultra-thin piezoresistive tactile sensor array using PAM/PEDOT:PSS hydrogel," 2017 14th Int. Conf. Ubiquitous Robot. Ambient Intell. URAI 2017, no. Cmc, pp. 950–955, 2017, doi: 10.1109/URAI.2017.7992873.
- [53] I. Babeli, G. Ruano, J. Casanovas, M. P. Ginebra, J. García-Torres, and C. Alemán, "Conductive, self-healable and reusable poly(3,4-ethylenedioxythiophene)-based hydrogels for highly

- sensitive pressure arrays," *J. Mater. Chem. C*, vol. 8, no. 25, pp. 8654–8667, 2020, doi: 10.1039/d0tc01947j.
- [54] W. Chen *et al.*, "High-strength, tough, and self-healing hydrogel based on carboxymethyl cellulose," *Cellulose*, vol. 27, no. 2, pp. 853–865, 2020, doi: 10.1007/s10570-019-02797-z.
- [55] S. Xu *et al.*, "Recent Advances in Flexible Piezoresistive Arrays: Materials, Design, and Applications," *Polymers (Basel).*, vol. 15, no. 12, 2023, doi: 10.3390/polym15122699.
- [56] M. Datta, "Design and Characterization of Crossbar architecture Velostat-based Flexible Writing Pad," no. June, 2023.
- [57] F. Pradas, V. Toro-Román, A. de la Torre, A. Moreno-Azze, J. F. Gutiérrez-Betancur, and M. Á. Ortega-Zayas, "Analysis of Specific Physical Fitness in High-Level Table Tennis Players—Sex Differences," *Int. J. Environ. Res. Public Health*, vol. 19, no. 9, 2022, doi: 10.3390/ijerph19095119.
- [58] R. R. Desai, P. S. Desai, N. R. Kulkarni, T. J. K. Palekar, and V. J. Steven, "Does Shoulder Girdle Strengthening Exercises have an Effect on Grip Strength in Adolescent Recreational Tennis Players? A Randomised Controlled Trial," *J. Clin. Diagnostic Res.*, 2021, doi: 10.7860/jcdr/2021/50314.15778.
- [59] A. Sánchez-Pay, J. Ramón-Llin, R. Martínez-Gallego, D. Sanz-Rivas, B. J. Sánchez-Alcaraz, and S. Frutos, "Fitness testing in tennis: Influence of anthropometric characteristics, physical performance, and functional test on serve velocity in professional players," *PLoS One*, vol. 16, no. 11, pp. 1–14, 2021, doi: 10.1371/journal.pone.0259497.
- [60] J. Fernandez-Fernandez, A. Ulbricht, and A. Ferrauti, "Fitness testing of tennis players: How valuable is it," *Br. J. Sports Med.*, vol. 48, no. SUPPL. 1, 2014, doi: 10.1136/bjsports-2013-093152.
- [61] J. Martinez-Cesteros, C. Medrano-Sanchez, I. Plaza-Garcia, R. Igual-Catalan, and S. Albiol-Pérez, "A velostat-based pressure-sensitive mat for center-of-pressure measurements: A preliminary study," *Int. J. Environ. Res. Public Health*, vol. 18, no. 11, 2021, doi: 10.3390/ijerph18115958.
- [62] "Adafruit Pressure-Sensitive Conductive Sheet (Velostat/Linqstat)." Accessed: Oct. 06, 2024. [Online]. Available: https://www.adafruit.com/product/1361#description
- "Staples Navigator Papel Impressora A4 Multiusos, Universal, 80 g/m², Branco, Resma." Accessed: Oct. 06, 2024. [Online]. Available: https://www.staples.pt/pt/pt/papel-multiusos-universal-a4-80-g-m-branco-469131
- [64] "VerdeLima Cortiça." Accessed: Oct. 06, 2024. [Online]. Available: https://www.verdelima.pt/product/cortica
- [65] "Saralon Electronics -Saral SilverH2O 600 Silver Based Conductive Ink." Accessed: Oct. 06, 2024. [Online]. Available: https://www.saralon.com/en/inks/electrically-conductive-inks:silver-based-ink:saral-silverh2o-600/
- [66] "Merchk Zinc chloride, Sigma Aldrich." Accessed: Oct. 06, 2024. [Online]. Available: https://www.sigmaaldrich.com/PT/en/product/sigald/208086
- [67] "Merchk Calcium chloride dihydrate, Sigma Aldrich." Accessed: Oct. 06, 2024. [Online]. Available: https://www.sigmaaldrich.com/PT/en/product/sigald/223506
- [68] "Merchk Calcium carboxymethyl cellulose, Sigma Aldrich." Accessed: Oct. 06, 2024. [Online]. Available: https://www.sigmaaldrich.com/PT/en/product/aldrich/419311
- [69] "Xerox ColorQube 8570/8580 Black Solid Ink Pack (4 Sticks)." Accessed: Oct. 06, 2024. [Online]. Available: https://www.shop.xerox.com/108r00930
- [70] "Note Rolo de Encadernamento de Livros." Accessed: Oct. 06, 2024. [Online]. Available: https://noteonline.pt/products/rolo-de-encadernamento-de-livros-2486987?srsltid=AfmBOorkZefMS-717c85MKD0V4K-5vhHysu2D-DBRIa90m3pnTXC3NdX

ANNEXES

A.1 Schematic: Structure of the smart grip

Figure 5.1 displays a schematic of the structure of the smart grips. The top and bottom layers act as the electrodes, with a 90° orientation from each other. The middle layer is the active layer, where the piezoresistive materials lay. It is also possible to observe what constitutes a single pixel in the pressure sensor array.

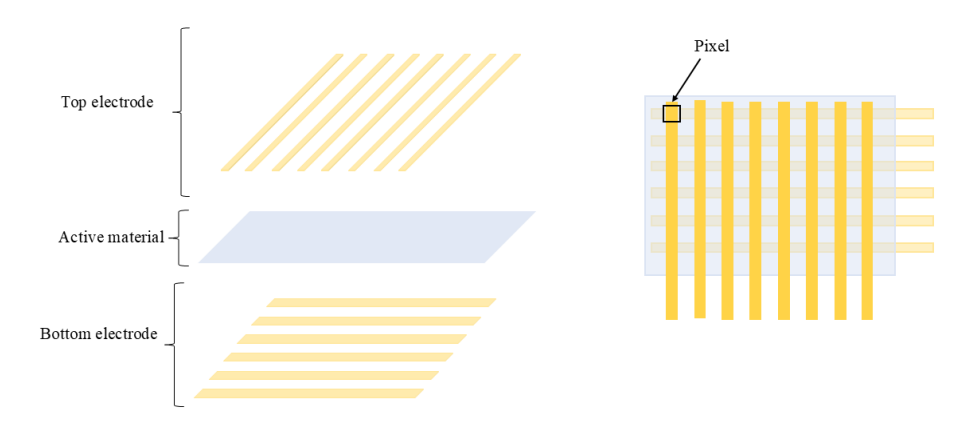


Figure 5.1 - Schematic of the structure of the grips.

A.2 Schematic: Implementation of the smart grip onto the racket

Figure 5.2 represents the implementation of the smart grip onto the racket. The racket's handle can be divided into two parts: the upper part where the shape of the handle is an octagonal prism and the lower part where the shape of the handle is trapezoidal prism. Since these two parts have different sizes and shapes, the grip needed to be split into two as seen in Figure 5.2.

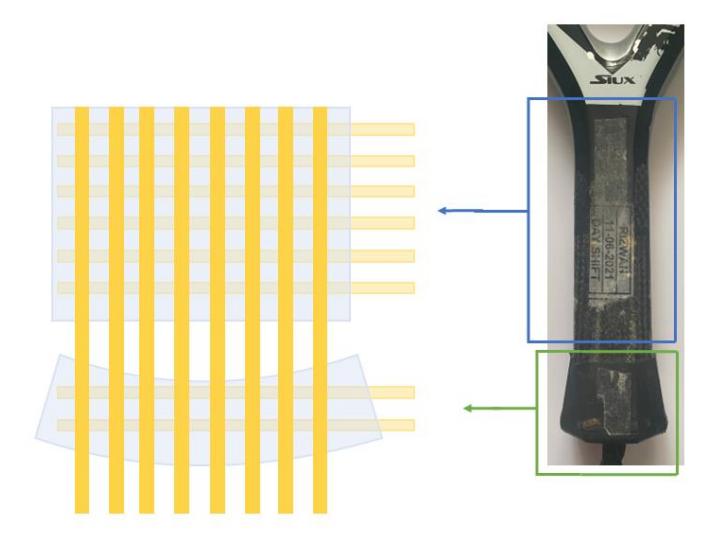


Figure 5.2- Schematic of the implementation of the grip onto the handle of the racket.

A.3 Mold for the hydrogel wells

Figure 5.3 shows the mold design for the hydrogel wells. This mold was printed in a wax printer to allow the hydrogel droplets to dry without the risk of spreading.

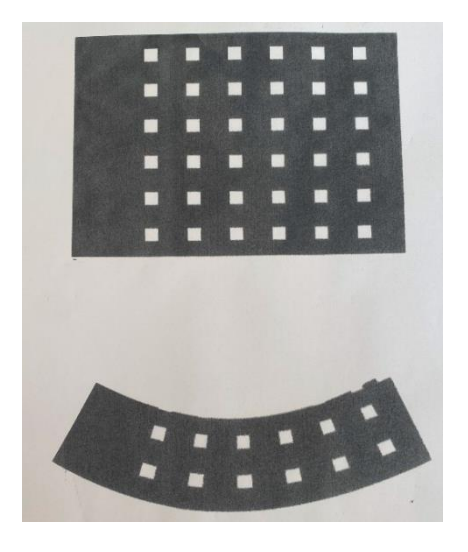


Figure 5.3 - Schematic of the mold used for the hydrogel wells.

A.4 Schematic: Connection of both parts of the PH grip

Figure 5.4 illustrates the connection between the two parts of the PH grip. A small hole was created in the lower section of the grip and filled with Ag ink. In the upper section, the Ag tracks were extended to establish a connection between both parts.

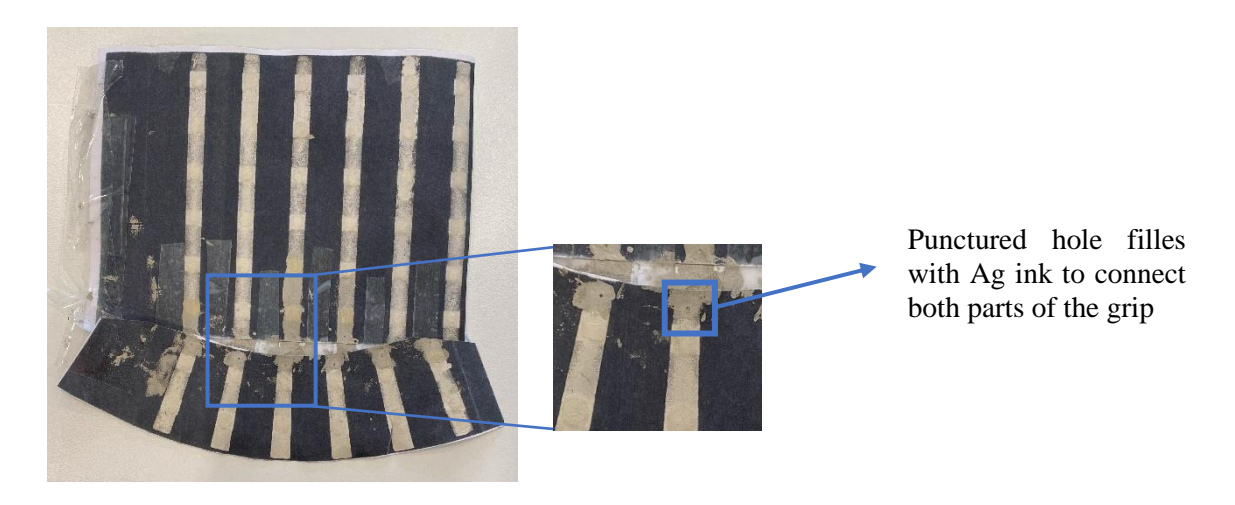


Figure 5.4 - Schematic of the connections of the two parts of the paper with hydrogel grip.

A.5 Schematic: Readout Circuitry

Figure 5.5 displays a schematic of the signal conditioning circuitry for the smart grips. This circuit remained consistent throughout the testing of all grips, with only the R_{bias} being exchanged.

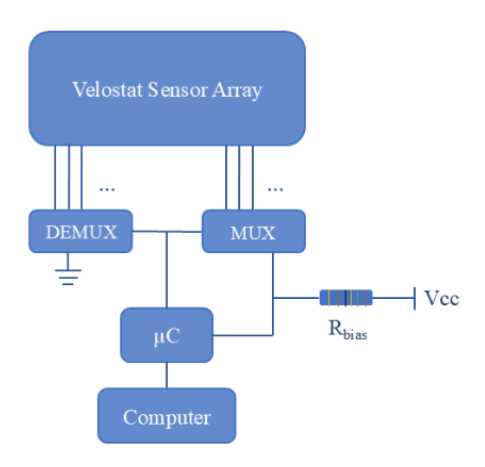


Figure 5.5 - Schematic of the readout circuitry for signal conditioning.

A.6 PV grip after testing

Figure 5.6 shows the PV grip after testing. As seen in the Figure below, some Ag electrodes were completely torn off , while others exhibited significant tears.



Figure 5.6 – State of the paper with Velostat grip after testing.

A.7 CV grip after testing

Figure 5.7 shows the CV grip after testing. As seen in the Figure below, this grip did not suffer any significant wear and tear.



Figure 5.7- State of the cork with Velostat grip after testing.

A.8 PH grip after testing

Figure 5.8 illustrates the PH grip after testing. This grip suffered wear and tear, being noticeable the deformation of grip.



Figure 5.8 – State of the paper with hydrogel grip after testing.

A.9 Calculations of the sensitivity values

Since the sensors are electrically resistive when no pressure is applied, then let's assume that the initial state is $F_0 = 100$ N. The corresponding pressure value is determined by the following Equation:

$$P = \frac{F}{A} \Longrightarrow P_0 = \frac{100}{\pi \times 2.5^2} \approx 50.929 \text{ Pa}$$

For the forces 250 and 500 N, the same process was applied:

$$P_{250} = \frac{250}{\pi \times 2.5^2} \approx 127.324 \text{ Pa}$$

$$P_{500} = \frac{500}{\pi \times 2.5^2} \approx 254.648 \text{ Pa}$$

Five pixels were selected for each grip to calculate the sensitivity. Initially, the resistance for each pressure was computed, followed by obtaining sensitivity values for each pixel. Subsequently, the average sensitivity of the whole sensor was calculated.

Using the PV grip as an example for the calculations, the sensitivity value was determined as follows. Pixel C exhibited the following output voltage values for each pressure.

- For P_0 , $V_{out} = 3.05 \text{ V}$
- For P_{250} , $V_{out} = 1.72 \text{ V}$
- For P_{500} , $V_{out} = 1.61 \text{ V}$

Therefore, resistance of the sensor for each output signal was determined with Equation (1). Recalling that R_{bias} of the PV grip was 330 Ω .

$$1.77 = \frac{R_0}{330 + R_0} \times 3.3 \Leftrightarrow R_0 = 381.765 \Omega$$

$$1.65 = \frac{R_{S \to P_{250}}}{330 + R_{S \to P_{250}}} \times 3.3 \Leftrightarrow R_{S \to P_{250}} = 330 \Omega$$

$$1.59 = \frac{R_{S \to P_{500}}}{330 + R_{S \to P_{500}}} \times 3.3 \Leftrightarrow R_{S \to P_{500}} = 306.842 \Omega$$

Equation (2) was used to determine the sensitivity for each section:

$$S_1 = \frac{\frac{330 - 381.765}{381.765}}{127.324 - 50.929} = -1.775 \text{ Pa}^{-1}$$

$$S_2 = \frac{306.842 - 381.765}{381.765} = -0.9634 \text{ Pa}^{-1}$$

As previously mentioned, the same calculations were applied to all five pixels of each grip, and the average of those sensitivity values was calculated to determine the sensor's overall sensitivity.

A.10 Calculations of the grips' prices

To determine the pricing of the grips, the cost of each material was analysed, and the final price of each component was calculated based on the quantity of material used.

Table 5.1 – Breakdown of the estimated prices of paper with Velostat, cork with Velostat and paper with hydrogel grips.

	Velostat layer	Paper substrate	Cork substrate	Ag ink	Hydrogel solution *2	Xerox wax	Adhesive paper	Estimated price/unit
Commercial price	4.51 € [62]	6.99 €/ 1 ream [63]	15.9 €/ roll [64]	2391.9 €/kg [65]	2.95 € / 7 mL [66]–[68]	189.3 €/4 sticks [69]	2.19 €/roll [70]	-
PV grip	0.76 €	0.0014€/sheet	-	0.337 € /0.1408 g	-	-	-	≈1.10€
CV grip	0.80 €	-	0.16€	1.09€	-	-	-	≈2.05
PH grip	-	0.0014 (x2)	-	0.337	0.61	0.022	0.10	≈1.01

^{*2 –} the pricing of the hydrogel solution was determined by the following calculations:

- 1 kg of Na-CMC costs 148 €. Since only 5 mL was used, it actually costed 0.52 €.
- 25 g of CaCl₂ costs 21.90 €. Since only 1 mL was used, it actually cost 1.82 €.
- 100 g of ZnCl₂ costs 21.50 €. Since only 1 mL was used, it actually cost 0.61 €.

Thus, the hydrogel solution costs 2.95 € per 7 mL. Since only 1.44 mL was used, the layer of hydrogel in the PH grip costs 0.61 €.



Margarida Laires